Mesenchymal Stem Cell-Derived Exosomes Versus its Conditioned Medium in Amelioration of Hippocampal Rat Model of Alzheimer's Disease, Behavioral, Biochemical, Histological and Immunohistochemical Study

Original Article

Dina Ali Maher Abdel Dayem[1], Amira Fathy Ahmed[1], Walaa Yehia Abdelzaher[2], Marwa Ibrahim Abdel Hamid[3], Fatma Khalil[4], Nashwa Fathy Gamal El-Tahawy[1], Seham Abdel Raouf Abd El-Aleem[1], Sara Mohamed Naguib Abdel Hafez[1]

[1]Department of Histology and Cell Biology, [2]Department of Medical Pharmacology, Faculty of Medicine, Minia University, Minia, [3]Department of Biochemistry, Faculty of Veterinary, Cairo University, Cairo, [4]Department of Animal and Poultry Management and Wealth Development, Faculty of Veterinary, Beni-Suef University, Beni-Suef, Egypt

ABSTRACT

Introduction: Alzheimer's disease is the most common form of dementia. Recently, mesenchymal stem cells-conditioned medium and exosomes have lately been employed in several therapeutic investigations.

Aim of work: To demonstrate hippocampus's biochemical, histological and immunohistochemical changes in albino rats after induction of Alzheimer and to evaluate the role of mesenchymal stem cells-conditioned medium versus exosomes on the albino rat Alzheimer model.

Materials and Methods: Thirty-two rats were used in this study plus ten rats were used in the preparation of mesenchymal stem cells derived conditioned media and exosomes. Rats were divided into four groups; Control, Alzheimer group, Conditioned media and Exosome treated group. Behavioral tests were performed. The hippocampi were prepared for biochemical, histological and immunohistochemical study.

Results: The Alzheimer group showed various behavioral changes. Rats also showed significant changes in hippocampal malondialdehyde, tumor necrotic factor, total antioxidant capacity, acetylcholine esterase and monoamine oxidase. Microscopically, hippocampi showed degenerated neurons as well as argyrophilic neurofibrillary tangles and amyloid plaque formation. The conditioned medium and exosomes treated groups displayed biochemical, functional and structural improvement with reduced argyrophilic neurofibrillary tangles and amyloid plaque formation. Treatment with exosomes was superior to conditioned medium as they improved neuronal function, regulated astrocyte and microglial activities and enhanced regenerative changes.

Conclusions: The conditioned medium and exosomes minimized Alzheimer - hippocampal associated biochemical, histological and immunohistochemical degenerative changes with better effect with exosome treatment. These results may pave the future for using exosomes as an effective adjuvant therapy in Alzheimer patients.

Key Words: Alzheimer's disease, conditioned medium, hippocampus, mesenchymal stem cell-derived exosomes, neurogenesis.

Revised: 10 June 2024, **Accepted:** 07 August 2024

Corresponding Author: *Dina Ali Maher Abdel Dayem*, *Department of Histology and Cell Biology, Faculty of Medicine, Minia University, Minia, Egypt,* **Tel.:** *+201021507617*, **E-mail:** *dina.ali@mu.edu.eg.*

ISSN: 1110-0559, December 2023, Vol. 7, No. 2.

INTRODUCTION

Alzheimer's disease (AD) is considered the most prevalent neurodegenerative disorder[1]. It accounts for 50 - 70 % of all dementia cases[2]. It is characterized by cognitive decline and memory failure. These deficits contribute to marked neuronal loss, glial cell malfunction, synaptic degeneration and brain atrophy[3].

The hippocampus is one of the first parts of the brain to be affected by AD[4]. It is characterized by extracellular accumulations of beta-amyloid (Aβ) protein and intracellular neurofibrillary tangles (NFTs) caused by abnormal hyperphosphorylation of the cytoskeletal tau protein[5].

There is no effective treatment for AD, despite the considerable attempts to understand its causes

 DOI: 10.21608/jmh.2024.296814.1129

and create therapeutic treatments[6]. Unfortunately, late treatment could cause irreparable brain damage within 1020- years after the onset of the disease, explaining the discrepancy with encouraging studies utilizing the AD animal models[7].

Stem cell-derived conditioned medium (CM) shows great potential to be produced as pharmaceuticals for regenerative medicine[8]. Several researches on secreted factors originating from stem cells indicated that these factors alone-not the stem cell itself-may assist tissue repair, hence it can be an alternate strategy for stem cell injection-based therapies[9]. Due to limitations on stem cell use in cell-based therapy, its CM, which contains exosomes, appears to be a viable and safer alternative with higher efficiency and fewer adverse outcomes[10].

Exosomes are micro-vesicles ranging in diameter from 30 to 100 nm and small lipid vesicles that are secreted by every type of cell. Exosomes derived from the mesenchymal stem cells can restore many tissue functions through their paracrine effect by secretion of growth factors, cytokines or chemokines[11].

Therefore, this experimental study aimed to demonstrate the biochemical, histological and immunohistochemical changes in the hippocampus of albino rats after induction of AD and to assess the role of MSCs-derived CM versus exosomes on albino rat AD model.

MATERIALS AND METHODS

In this current study, forty-two male albino rats were employed. The experimental groups included thirty-two 68- weeks adult rats of weights ranging from 150 - 200 g. In addition, ten male albino rats of 4 - 6 weeks weighing 70 - 80 g were used to prepare mesenchymal stem cells-derived conditioned media and exosomes.

This study was performed in accordance with the local guidelines of the ethical committee of the Faculty of Medicine, Minia University, Egypt for the use of laboratory animals. Approval No.45: 2021 according to the international guidelines (Act 1986).

Preparation of rat's Alzheimer disease model:

Alzheimer's like disease was induced in adult male albino rats by aluminum chloride (AlCl3) (Sigma-Aldrich, Egypt) (100 mg/kg) dissolved in distilled water was administered by a gastric tube at a dose of 0.5 ml/100 g daily for 42 days[12].

Isolation and Culture of Bone Marrow derived Mesenchymal Stem Cells (BM-MSCs):

After halothane anesthesia[13] and skin sterilization, dissection of rats' femurs and tibiae was done then were rinsed in phosphate buffer saline (PBS) (Hyclone, USA) in a Petri plate and flushed with Dulbecco's Modified Eagles Medium (DMEM) (Lonza, Belgium). Nucleated cells were isolated using a Ficoll/Paque density gradient (Pharmacia), then cultured in 20 ml complete media (Lonza, USA) and incubated at 37°C in a 5 % humidified CO2 incubator (Shellab, USA) for 7 - 10 days. Daily examination of the cultured cells was done using an inverted microscope (Olympus CKX41, USA). Following that, the second media exchange was completed in 3 - 4 days. It takes 34- weeks for the cells to reach confluence (80 - 90 %). The media changes 2 times per week. Washing with PBS was done and trypsinization was performed by using 1 - 2 ml of 0.25 % trypsin in 1 mM EDTA (Lonza, Belgium) for 5 minutes at 37°C. The cells were next tested with 5 ml of complete media after trypsinization had been stopped[14].

Obtaining the conditioned medium (CM):

Conditioned medium was prepared from the third to fifth passages of BM-MSCs as follows:

MSCs (2x106) were cultured with 2 ml FBS-free DMEM for 48 hours. The CM was obtained after aspiration in Eppendorf tube then filtered with 0.20 um sterile syringe filter (CORNING, NY14831, Germany). The components of complete media; Dulbecco's Modified Eagle's Medium (89 mL) (Lonza Company, Switzerland). 10 % foetal bovine serum (FBS) - 10 mL (Lonza Company, Switzerland). Antibiotics: 100 U/ml penicillin, 100 µg/ml streptomycin[15].

Isolation and characterization of BM-MSCs derived exosomes:

Exosomes were isolated from the supernatants of third passage MSCs grown overnight in RPMI medium (Roswell Park Memorial Institute medium) without FBS.They were obtained after differential centrifugation at 30009 g to eliminate cells and then 10,000 x g for 20 min to remove debris. Cell-free supernatants were centrifuged at 100,000 x g

(Beckman Coulter Optima L-90 K ultracentrifuge) for one hour at 4 °C, then washed in 25 mM of serum-free medium 199 containing N-2-Hydroxy Ethyl Piperazine-N'-2Ethane Sulfonic acid (HEPES) (Sigma) and then a 2nd ultracentrifuge in the same conditions was performed.

Exosome pellets were obtained in 100 µL distilled water and stored at -80°C before injection. The protein content of exosomes was measured using the Lowry Protein Assay Kit (Bio Basic)[16].

For characterization, exosomes were washed and exposed to 2.5 % glutaraldehyde for two hours. The samples were ultracentrifuged and suspended in 100 µL of human serum albumin. Exosomes (20 µL) were put onto a formvar/carbon-coated grid and negatively stained with aqueous phosphor-tungstic acid 3 % for one minute and viewed by TEM (Figure 1a1, a2).

For flow cytometric characterization of exosomes[17]; exosomes were stained with 10 µl of antibody (CD83 PE and CD61 PE) for 20 minutes at room temperature (Figure 1b1, b2). After adding 2 ml of PBS to the exosomes, they were centrifuged at 200 g for 5 minutes at room temperature and the supernatant was discarded. Exosomes were resuspended in 0.5 ml of flow buffer (5 % FBS + 95 % PBS).

Analysis was done using a Coulter Elite XL Caliber flow cytometer, which collected 10,000 events (Figure 1b). Regarding in vitro labeling of exosomes with PKH-26 fluorescent dye, exosomes were collected during MSCs' third passage and were labeled with PKH26 fluorescent linker dye (Sigma-Aldrich, Saint Louis, USA)[18].

Experimental design:

The experimental groups included thirty-two rats. They were equally divided into four groups; Control group (C- group): rats received the vehicle (distilled water) orally via gastric tube for 42 days at a dose of 0.5 ml/100g body weight. AD- group (Alzheimer group): rats were daily administered AlCl3 100 mg/kg dissolved in distilled water at a dose of 0.5 ml/100 g via a gastric tube for 42 days[12]. CM-treated group (Conditioned media group): rats were daily given AlCl3 at the same dose and duration as AD-group, then after 24 hours, rats were injected with 0.5 ml conditioned medium through rats' tail vein once under ether inhalation anesthesia[19], then, rats were sacrificed after 4 weeks. Exo-treated group (Exosome treated group): rats received AlCl3 daily as in the AD-group then given a single injection of 100 µg MSCs-derived exosomes suspended in 1ml phosphate buffered saline through the rats' tail vein under ether inhalation anesthesia[20], then rats were sacrificed after 4 weeks.

Behavioral tests:

The following behavioral tests were performed to evaluate rats' activity and memory changes in AD model and the therapeutic effect of CM/MSCs derived exosomes. Five rats from each group were subjected to the test. These tests were performed on each rat separately at 3-time points; after 42 days of AlCl3 administration (Day zero) and after 2 weeks and 4 weeks after treatment with CM/MSCs-derived exosomes administration.

• Open Field test:

This test was used to assess locomotor activity, exploration and anxiety[21]. The rat was put into one of the four corners of the open field and then was allowed to explore the field for 5 minutes. For each animal, locomotion anxiety-like behaviors (Number of peripheral squares crossed with all 4 paws and rearing; the frequency with which rat stands against the wall of the maze), freezing (immobility) time and exploration (number of center square entries with all four paws and time spent in them) were measured (Figure 1d).

• Learning and memory Tests:

o Y-Maze test.

This test was carried out to analyze spatial short-term working memory by estimating the spontaneous alternative behavior in maze arms[22]. Arms were labelled as A, B and C; then, each rat was put at the start of the (A) arm and left for 8 minutes. The maze arm entry sequence was calculated using overlapping triplet sets (i.e., ABC-CBA-ABC). The proportion of spontaneous alternation behavior (SAP) was evaluated in the Y-maze to assess working memory (Figure Id).

$$SAP = \frac{\text{actual alternation}}{\text{maximum alternation (total arm entries} - 2)} \times 100.$$

o Novel Object Recognition test (NOR)

This test was carried out to assess short-term memory. A novel object recognition test was used to detect learning and memory deficits depending on

rat's natural behavior in exploring new items more than familiar ones, that is known as recognition memory according to the procedure demonstrated by[23]. NOR was assessed by calculation of the discrimination index (DI) (Figure 1c).

$$\text{Discrimination index (DI)} = \frac{\text{time exploring the novel object}}{\text{total time exploring both novel and familiar objects}}$$

At the time of sacrifice, rats were anesthetized by ether inhalation[13]. The whole brain tissues were obtained for paraffin sections Each brain was sagittally divided. The right side was processed for electron microscope study while the left side was used for biochemical study.

Biochemical study:

The left hippocampal tissue was homogenized in 10mM (pH 7.4) potassium phosphate buffer. The ratio of tissue weight to homogenization buffer was 1:10. Centrifugation was done at 4000 g for 10 min at 4 C°. The supernatants were used for the assessment of:

a) Malondialdehyde (MDA); a reactive aldehyde was used as measure of lipid peroxidation (marker for lipid peroxidation).

b) Total Antioxidant Capacity (TAC), a marker for the oxidative stress. TAC was measured calorimetrically by kits obtained from Biodiagnostic, Egypt. TNF-α was measured by ELISA kit (Elabscience, USA).

c) Tumor necrotic factor (TNF-α), a marker for inflammation.

TAC and TNF-α were detected according to their commercial kits. MDA level was detected according to[24].

d) Gene expression analysis of acetylcholine esterase (AChE).

e) Monoamine oxidase (MAO) m-RNA RNA isolation and reverse transcriptase reaction were also evaluated.

The Biospin RNA Extraction Kit (Bioflux, China) was used to extract total RNA from 50 mg of hippocampus tissue, as directed by the manufacturer. NanoDrop (Thermo Scientific, USA) was used to analyze both the purity and concentration of RNA[25]. The first strand of cDNA was synthesized based on the manufacturer's instructions using reverse transcriptase (Biobasic, Canada). Regarding quantitative real time PCR, BioEasy's SYBR™ Green qPCR Master Mix was used for its quantitative. The cDNA was amplified using 40 cycles of denaturation (95 °C for 45 s), annealing (60 °C for 45 s) and extension (72 °C for 45 s). The primer pairs utilized are shown in Table 1. The size of all amplicons was assessed by agarose (2 %) gel electrophoresis with SYBR DNA dye (Invitrogen™ gel). Each measurement was done 3 times, with β-actin serving as an internal control[26]. The reaction was carried out in an iQ5 iCycler thermal cycler (Bio-Rad, Germany). All experiments included cDNA template-negative samples. The melting curves of the primer sets were examined. Relative quantification of mRNA was detected via normalized fold change technique[27].

Table 1: The mean levels of locomotor and anxiety like behaviors in the studied:

Behavior	Zero day		Second week				Fourth week			
Locomotor behavior	C- group	AD-group	C- group	AD-group	CM-group	Ex-group	C- group	AD-group	CM-group	Ex-group
Number of crossed peripheral squares	42.0 ± 20	15.0 ± 2.0**	35.0 ± 12.7	13.8 ± 3.1**	12.8 ± 3.7**	13.6 ± 5.1**	39.0 ± 13.8	13.8 ± 6.3**	18.0 ± 5.7**	27.8 ± 9.9*
Rearing frequency	7.80 ± 4.65	0.60 ± 0.54**	8.8 ± 4.5	3.4 ± 2.3**	3.0 ± 1.5*	5.4 ± 2.0	8.6 ± 4.15	1.0 ± 0.7**	2.2 ± 0.8**	1.4 ± 0.5**
Anxiety-like behavior										
Freezing time/ second	101.0 ± 21.0	241.0 ± 36.1**	137.2 ± 36.4	299.8 ± 49.0**	261.4 ± 23.4*	218.0 ± 27.7*	150.0 ± 75.2	281.0 ± 52.4**	280.0 ± 41.8*	178.0 ± 30.3
Grooming duration/ second	33.8 ± 13.3	96.0 ± 13.8**	11.0 ± 6.5	43.8 ± 27.2**	40.4 ± 15.1*	17.2 ± 11.6	45.0 ± 14.0	116.7 ± 26.5**	53.7 ± 9.50	36.8 ± 7.9

Biochemical analysis was done at the Pharmacology Department, Faculty of Medicine, Minia University, Egypt and Biochemistry and Molecular Biology Department, Faculty of Veterinary Medicine, Cairo University, Egypt.

Histological and immunohistochemical study:

For light microscopic examination, whole brain tissue samples were fixed in 10 % buffered formalin, then sagittal sections were done and processed to produce paraffin blocks. Serial 5 µm tissue sections were stained with:

• Hematoxylin and eosin (H and E)[28].

• Modified Bielschowsky's silver method[29].

Immunohistochemical staining was performed to the following according to manufacturer's instruction using:

• anti-glial fibrillary acidic protein (GFAP); a marker for astroglia activation (Abcam, ab10062, UK), monoclonal mouse antibodies.

• Anti-nestin antibody; a marker for stem cells and progenitor cells, which is a midway stage between stem cells and fully differentiated adult neural cells (Abcam, ab22035, UK), monoclonal mouse antibodies.

• Anti-CD86 antibody; a marker for classically activated proinflammatory microglia (Thermo fisher scientific, PA5 - 88284, UK), rabbit polyclonal antibody.

• Anti-CD163 antibody; a marker for alternatively activated or anti-inflammatory macrophages (Thermo fisher scientific, MA5 - 11458, UK), monoclonal mouse antibodies.

Positive controls:

The changes in the immunohistochemical reaction of the brain tissues of the treated animals were detected through a comparative examination of the corresponding tissues of the normal control animals.

• The positive control for both anti-nestin and anti GFAP antibodies were the normal brain tissue of the normal control animals themselves.

• The positive control for anti- CD 86 and anti-CD163 antibodies were the normal tonsil tissue of

the normal control animals themselves (figures were not included).

In negative controls slides:

The same technique was applied but the primary antibody was not added (figures were not included).

Sections were counterstained with hematoxylin, dehydrated, cleared and then mounted. The reaction was identified as brownish cytoplasmic granules. J.

Transmission electron microscopic study:

Ultrathin sections were prepared according to Weil and his colleagues[30]. Fixation of small pieces of the right hippocampi (mm^3) were immediately fixed in 2.5 % glutaraldehyde in 0.1 M cacodylate buffer at pH 7.4 at 4 Co for 24 hours, then, washed with buffer and postfixed in 1 % osmium tetroxide in distilled water for 2 hours Specimens were dehydrated with increasing concentrations of ethanol and embedded in epoxy resin. Ultrathin sections (70 - 80 nm-thick) were cut using diamond knives using the Leica EM UC6 ultramicrotome, mounted on grids, stained with uranyl acetate and lead citrate, then examined by the transmission electron microscope in the Central Lab, Minia University's Microanalysis and Nanotechnology.

Image capture:

PKH26 labeled exosomes were captured by LC-6 USB3.0 colorful CMOS digital camera (LABOMED, USA) and examined using a green filter (Alexa Fluor 488 nm) of the fluorescence microscope (LABOMED Fluorescence microscope LX400, catalog No. 9126000, USA) in Global Labs - Medical Labs, Unit # 403, Medical Centre II, 3 Mahmoud Fathy St., 9th district, Nasr City, Cairo 11528, Egypt.

H and E, Modified Bielschowsky's silver method, immunohistochemical and semithin staining sections were captured using a high-resolution color digital camera placed on a BX51 microscope (Olympus, Japan), connected to a computer programmed with LC micro application software in the Histology and Cell Biology Department, Faculty of Medicine, Minia University, Egypt. Ultrastructural images were captured using transmission electron microscopy (JEM-100CX II; Japan) at the Central Lab for Microanalysis and Nanotechnology, Minia University, Egypt.

Morphometric measurements:

Morphometric study were done in 5 successive non-overlapping fields/sections for each rat hippocampus in each group at magnification × 400. The following parameters were detected:

• Degenerative neurons (shrunken darkly stained) in the hippocampus proper (Cornu Ammonis) were manually counted from H and E-stained sections.

• NFT-containing cells were manually counted from silver-stained sections in Cornu Ammonis and DG.

• The mean number of CD86-positive microglial cells were manually counted.

• The mean surface area fraction of GFAP, nestin and CD163 (Image J (http://rsbweb.nih.gov/ij/; NIH, Bethesda) was used to assess these parameters).

Statistical analysis:

• The quantitative data were analyzed using Graph Pad Prism (Graph Pad Software, San Diego, California, USA, Version 9.01 for Windows, www.graphpad.com). Each group's parameters had their mean and standard error of mean (SEM) computed. Data were presented as means ± SEM. To find significant differences between several groups, the one-way (ANOVA) test was employed, followed by post-hoc Tukey analysis. The student t-test was used to compare the differences between two groups. Statistically significant results were assessed when the *p*-values were < 0.05 and non-significant when the *P*-values were > 0.05.

RESULTS

The mean level of spontaneous alternation behavior percentage:

Throughout this study, the Alzheimer (AD) group rats exhibited a significantly lower spontaneous alternation behavior percentage (SAP) than the control (C) rats. In the second week, the conditioned media (CM) and exosome (Exo) treated groups had a significantly lower SAP than the C group ($p = 0.0014, 0.0346$) but not the AD group. At the end of the study (4th week), the CM-treated group was considerably ($p = 0.0011$) lower than the C group, but not significantly different from the AD group. However, SAP in the Exo-treated

group was comparable to that of the C group and significantly lower than that of the AD group ($p = 0.0073$) (Figure 2a).

The mean level of discrimination index (DI):

During the experiment, AD-group animals showed a significantly lower discrimination index (DI) than control rats. Comparing the treated groups, in the second week; CM-treated demonstrated substantial decreases in DI compared to the C group ($p = 0.0006$) but not to the AD group. While Exo-treated groups showed a substantial increase in DI when compared to the AD group alone ($p = 0.0361$). At the end of the study (4^{th} week), DI in the CM-treated group was significantly higher than in the C and AD groups ($p = 0.0001$ and $p = 0.0101$, respectively). The DI of the Exo-treated group was similar to that of the C group and significantly greater than the AD group ($p < 0.0001$) and CM-treated groups ($p = 0.0208$) (Figure 2b).

• *Open field test result:*

Table 1 showed the changes in locomotor and anxiety-like behaviors seen in rats during the open-field test. During the experiment, the AD-group had significantly lower activity levels (peripheral squares crossed by rats and rearing frequency) and anxiety-like behaviors (freezing and grooming duration) than the C-group ($p < 0.01$). In the second week, the CM-treated group had a significantly higher number of crossed peripheral squares and rearing frequency ($p < 0.01$ and 0.05, respectively). Moreover, the CM-treated group spent significantly longer ($p < 0.05$) freezing and grooming duration than the control group. The Exo-treated group had a substantial drop ($p < 0.01$) in the number of crossed peripheral squares, but no significant decrease in rearing frequency. The Exo-treated group had significantly longer frozen time ($p < 0.05$) but no significant increase in grooming duration.

Biochemical results:

The AD group showed considerably greater levels of hippocampal malondialdehyde (MDA) (nmol\g) than the control group ($p < 0.0001$). Treatment with CM and exosomes significantly reduced MDA levels in the hippocampus compared to the AD group (both $p < 0.0001$), however, no significant differences were observed when compared to the control group. Additionally, there was no significant change between the CM and Exo-treated groups (Figure 3a).

The AD group had a significantly lower total antioxidant capacity (TAC) (mmol\g) level compared to the C group ($p < 0.0001$). While the treatment of CM and exosomes significantly increased TAC levels in the hippocampus compared to the AD group ($p = 0.0003$, 0.0002), there were no significant differences in TAC levels when compared to the control group. Also, there was no significant change between the CM and Exo-treated groups (Figure 3b).

The AD group showed significantly higher TNF-α levels (pg/mg) compared to the control group ($p < 0.0001$). CM/exosome treatments significantly reduced TNF-α levels in the hippocampus compared to the AD group (both $p < 0.0001$), with insignificant alterations when compared to the control group or to each other (Figure 3c).

The AD group had significantly lower levels of acetylcholineesterase (AChE) expression compared to the control group ($p < 0.0001$). CM/exosomes treatments significantly enhanced AChE levels in the hippocampus compared to the control and AD groups (both $p < 0.0001$). There was a significant difference between the CM and Exo-treated groups ($p < 0.0001$) (Figure 3d).

The AD group had significantly lower monoamine oxidase (MAO) expression levels compared to the C group ($p < 0.0001$). CM/exosomes treatments significantly increased MAO levels in the hippocampus compared to the control and AD groups (both $p < 0.0001$). A significant difference was noticed between the CM and Exo-treated groups ($p < 0.0001$) (Figure 3e).

Histological and immunohistochemical results:

Confirmation of homing of labeled exosomes in hippocampal tissue

The injected exosomes labeled with PKH26 were detected in rat hippocampal tissue of Exo-treated group using a fluorescent microscope (Figure 1e).

Hematoxylin and eosin (H and E):

H and E sections of the hippocampus proper and the dentate gyrus (DG) of the C group revealed that the hippocampus proper was composed of the Cornu Ammonis (CA) and its components, CA1, CA2, CA3 and CA4 regions. Cornu ammonis was showed laminar organization comprising numerous strata, including stratum oriens (so), stratum pyramidalis (sp), stratum lucidum (sl), stratum radiatum (sr) and stratum lacunosum-molecular. The DG looked like a black V-shaped structure encircling the CA4 region with an open section. It consisted of three layers: molecular, granule and polymorphic cell

layers, which were visible on both sides of the CA4 area. The supra-pyramidal and infra-pyramidal blades meet at the crest of DG (Figure 4a). The CA1 area was formed of dense, evenly arranged 3 - 4 compact rows of small pyramidal neurons, with little neuropil between. Each pyramidal cell formed of a single, rounded, central, vesicular nucleus with prominent nucleoli (Figure 4b). CA3 and CA4 areas consisted of a substantial number of pyramidal neurons. The neurons had single, rounded, central and vesicular nuclei with visible nucleoli. The nuclei of sparse neuroglial cells were dark basophilic stained, small, spherical and distributed over a pink neuropil background. The neuropil was formed up of neuronal and glial cell processes (Figure 4c, 4d). The DG revealed dense columns of granular cells, forming a rounded layer with vesicular nuclei and little interstitial tissue between these neurons. Scattered neuroglial cells were found on a pink neuropil (Figure 4e).

The AD group showed pyramidal neuron heterogeneity in CA1, CA3 and CA4. The majority of the small and the large pyramidal neurons showed significant degeneration. Pyramidal neurons exhibited widely separated shrunken cell bodies, pericellular haloes and strongly stained pyknotic nuclei. While other degenerated cells exhibited karyolysis. Congested blood capillaries were also present. A few pyramidal cells were normal, with basophilic cytoplasm and large central round vesicular nuclei (Figure 5a - 5c). DG revealed several shrunken granular cells with highly pigmented basophilic cytoplasm and pyknotic nuclei. Some granular cells were surrounded by pericellular haloes and had vacuolated cytoplasm or absence of cytoplasm all (Figure 5d). Glial cells occurred on a pink neuropil in all areas of the hippocampus in this group (Figure 5a - 5d). Both CA3 and CA4 appeared to be the most affected areas.

The CM-treated group showed some improvement in histological alterations induced by AD, which were more specific to CA1, CA3 and DG. The majority of pyramidal cells in CA1 and CA3 had normal morphology with vesicular nuclei, although a few were shrunken with deeply stained nuclei (Figure 6a, 6b). While CA4 regions exhibited few pyramidal cells with deeply stained nuclei (Figure 6c). It was noticed in DG that the majority of the granular cells contained vesicular nuclei, Cytoplasmic NFTs were seen in few dispersed neurons appeared. Vacuolated neuropil in the sub-granular zone was seen (Figure 6d). Exo-treated group demonstrated amelioration of all previously reported histological alterations that occurred in AD-group and showed more improvement than CM-group. Most of the pyramidal neurons in CA areas appeared normal, with basophilic cytoplasm and vesicular nuclei. However, a few scattered degenerated pyramidal neurons with shrunken cell bodies, pyknotic nuclei and perineural halos were observed (Figure 7a - 7c). Granular cells in DG retained their typical appearance, including basophilic cytoplasm, vesicular nuclei and little vacuolation in the sub-granular zone (Figure 7d). Glial cells were seen on a pink neuropil in all areas (Figure 7a - 7d).

Bielschowsky's silver stain:

Sections of the CA1 and CA4 areas of the C group's hippocampus proper revealed pyramidal neurons with faintly stained nuclei and large darkly stained nucleoli. The cytoplasm and the axons were lightly stained (Figure 8a, 8b). The granular neurons in DG had lightly stained nuclei and prominent nucleoli (Figure 8c). In AD-group sections, intra-neuronal aggregations of argyrophilic NFTs were seen in cells from the CA1, CA4 and DG areas. NFTs developed as an accumulation of argyrophilic neurofibrils, which were primarily seen in neuronal cell bodies and the proximal parts of axons. Pyramidal cell nerve fibers were also degenerated and darkly stained (Figure 8d, 8e). The DG included several undersized, degenerative granular neurons with large NFTs (Figure 8f). Amyloid plaques were identified as huge, extracellular aggregates of spherical golden-brown clumps. Two types of plaques were detected; dense core plaques, which had a thick amyloidogenic core (Figure 8g) and diffuse plaques with no core (Figure 8h). Thinning of degenerated nerve fibers was also observed (Figure 8i).

In the CM-treated group, most pyramidal neurons in CA1 and CA4 had lightly stained nuclei and intact lightly stained axons, while other neurons were smaller, with accumulated argyrophilic NFTs in their cytoplasm, obscuring their nuclei and proximal axons. However, few well-stained axons appeared, degraded or segmented (Figure 9a, 9b). The DG exhibited preservation of most granular neurons, but some shrunken degenerated granular cells with cytoplasmic NFTs were noticed (Figure 9c). Furthermore, the Exo-treated group showed more preservation of the normal structure with less degeneration of pyramidal neurons in CA1 and CA4 than the CM-treated group. Only a few shrunken neurons had intra-neuronal argyrophilic NFTs in their cytoplasm, which masked their nuclei and proximal axons. A few deeply stained degenerated nerve fibers were also seen (Figure 9d, 9e). Most granular neurons in the DG in were also preserved, some scattered granular

cells were shrunken and degenerated with intracytoplasmic NFTs (Figure 9f).

Immunohistochemical results:

The control group showed normal distribution of immunohistochemical expression for glial fibrillary acidic protein (GFAP) in the form of mild positive cytoplasmic reaction in the astrocytes and their processes in stratum oriens, stratum radiatum and between the pyramidal neurons of the stratum pyramidalis in CA region. GFAP expression was detected in the molecular layer, pleomorphic layer and in between the granular cells of the granular cell layer in DG region. The immuno-reactive astrocytes appeared as star-shaped cells with thin processes (Figure 10a, 10b) while there were more strongly GFAP positively stained astrocytes in AD group with prominent ramified cytoplasmic processes when compared to the control group in stratum oriens, stratum radiatum and in between the pyramidal neurons of the stratum pyramidalis in CA region. It was also noticed in the molecular and pleomorphic layers and between the granular cells of the granular cell layer in DG region (Figure 10c, 10d).

CM-treated group showed slightly decreased GFAP immuno-reactivity in enlarged astrocytes with prominent ramified cytoplasmic processes compared to AD-group that were noticed in stratum oriens, stratum radiatum and in between the pyramidal neurons of the stratum pyramidalis in CA region as well as in molecular layer, pleomorphic layer and in between the granular cells of granular cell layer in DG region (Figure 10e, 10f).

Exo-treated group showed few lightly stained GFAP immuno-reactive astrocytes compared to the AD-group and the CM-treated groups. These astrocytes were noticed in stratum oriens, stratum radiatum and between the pyramidal neurons of the stratum pyramidalis in the CA region and in the molecular layer, the pleomorphic layer and between the granular cells of the granular cell layer in DG region (Figure 10g, 10h).

Regarding nestin antibody, the C group showed nestin immune-positive reaction in granular cells of DG, while other cells had no or faint cytoplasmic expression (Figure 11a). Meanwhile AD-group exhibited faint nestin reaction in granular cells (Figure 11b). It was noticed in the CM-treated group more nestin expression in more granular cells as compared to AD-group (Figure 11c). Exo-treated group showed obvious increase in nestin reaction in more granular cells compared to both AD and CM groups (Figure 11d).

Anti-CD163 antibody showed positive immunostaining, in the control group in the form of cytoplasmic expression in some microglial cells in hippocampus proper and DG (Figure 12a, 12b). While AD-group displayed a decrease in CD163 immune-positivity in the microglial cells compared to C-group that had faint expression (Figure 12c, 12d). It was noticed in CM-treated group increased CD163 immune-positive microglial cells as compared to AD-group (Figure 12e, 12f). The Exo-treated group showed an apparent increase in anti-CD163 antibody cytoplasmic expression intensity (Figure 12h, 12i) as compared to both AD and CM groups in numerous microglial cells which tend to aggregate in close proximity to blood capillary (Figure 12g).

Regarding CD86, the control group showed positive immunostainning for anti-CD86 antibody in the form of cytoplasmic expression in scattered microglial cells in the hippocampus proper and the DG (Figures 13a, 14a and 14b). The AD-group showed more CD86 positive microglial cells compared to C-group. Positive glial cells had densely immunostained cytoplasm (Fig. 13b, 14c and 14d). The CM group showed few microglial cells with positive cytoplasmic expression for CD86 antibody compared to AD-group (Figures 13c, 14e and 14f). Exosomes-treated group showed more reduction in CD86 positive glial cells compared to both the AD and the CM groups (Figures 13d, 14g and 14h).

Ultrastructural results:

Ultrastructurally, the pyramidal neurons in the control rat hippocampus revealed large rounded central vesicular nuclei with prominent nucleoli. Their cytoplasm contained a well-developed rough endoplasmic reticulum (rER), many mitochondria and 1ry lysosomes (Figure 15a, 15b). The cytoplasm of the microglia appeared electron lucent and their nuclei were elongated with peripheral heterochromatin. They exhibited typical lengthy stretches of endoplasmic reticulum with cytoplasmic vacuoles (Figure 15c, 15d). The astrocytes showed rounded large heterochromatic nucleus surrounded by scanty cytoplasm containing some organelles like mitochondria and rER (Figure 15e). Several myelinated axons with smooth regular contour and compact myelin lamellae were distinguished. The axoplasm of these axons contained intact mitochondria (Figure 15f).

The AD-group showed two forms of neuronal damage. The first appeared in some degenerated pyramidal neurons which were shrunken and contained and the chromatin in their nuclei was

condensed peripherally and surrounded with scanty vacuolated cytoplasm that lost some cytoplasmic organelles and intracytoplasmic vacuolations, these neurons were surrounded by edematous damaged neuropil (Figure 16a, 16b). The second form of degeneration appeared in the pyramidal neurons that contained electron dense cytoplasm bordered by notched cell membrane and contained dark heterochromatic eccentric nuclei. The cells were surrounded by vacuolated neuropil. The electron-dense cytoplasm showed dilated rER cisternae, intracytoplasmic vacuolations and 2ry lysosomes engulfing myelin like figures (Figure 16c). This group showed change of morphological features of microglia. There were elongated microglia with electron dense cytoplasm with multiple intracytoplasmic vacuoles, 1ry and 2ry lysosomes. It also appeared as dark dystrophic microglia which exhibited electron dense cytoplasm and extensive nuclear chromatin condensation with microglial processes surrounding degenerated neurons. Edematous damaged neuropil was also noticed surrounding the microglia (Figure 16d, 16e).

Astrocytes in this group showed irregular nuclei with less electron dense nuclear chromatin, vacuolated cytoplasm with engulfed myelin, dilated cisternae of rER, remnants of microfilaments and damaged mitochondria with disrupted cristae (Figure 17a, 17b). Many myelinated degenerated axons were observed; some of them showed irregular outline, large axoplasmic vacuoles and decompacted myelin lamella and others exhibited areas of thinning or focal interruption of myelin sheath and disruption of the neurofilaments (Figure 17c, 17d).

In the CM-treated group, the pyramidal neurons acquired many morphological forms; some neurons contained areas of empty cytoplasm and their nuclei were euchromatic with dense peripheral chromatin. Their cytoplasm displayed dilated cisternae of rER, 2ry lysosomes with myelin-like figure and damaged mitochondria with disrupted cristae (Figure 18a, 18b). Other neurons appeared with electron-dense cytoplasm and dark heterochromatic nucleus, notched cell membrane. They were surrounded by vacuolated neuropil. Their cytoplasm showed 1ry lysosomes, 2ry lysosomes, intracytoplasmic vacuolations, dilated cisternae of rER and myelin-like figure (Figure 18c). On the other hand, some neurons appeared more or less normal with vesicular nuclei (N) and dispersed chromatin. Their cytoplasm showed apparently intact organelles except for some dilated rER cisternae (Figure 18d). Dark elongated microglia and their processes exhibited electron-dense cytoplasm with numerous 1ry lysosomes and multiple cytoplasmic vacuoles; some contained engulfed myelin (Figure 18e). Microglia were seen in close vicinity to the degenerated axons and astrocytes (Figure 18f). Astrocytes showed irregular nuclei with electron-dense nuclear chromatin, areas of empty cytoplasm, engulfed myelin, dilated cisternae of endoplasmic reticulum, 2ry lysosomes and some apparently intact mitochondria and others appeared damaged with disrupted cristae (Figure 19a, 19b). Myelinated degenerated axons were also present. Some axons had irregular outlines; axoplasmic vacuoles and disrupted neurofilament. Few areas exhibited decompacted myelin lamella, others showed areas of thinning and focal interruption of myelin sheath (Figure 19c, 19d). However, some axons in this group revealed compact myelin lamellae and small axoplasmic vacuoles could be noticed (Figure 19d). The pyramidal neurons of Exo-treated group were more or less normal if compared to the C-group. They showed large rounded central vesicular nuclei with dispersed chromatin and prominent nucleolus. Its cytoplasm showed intact mitochondria and 1ry lysosomes except for some dilated rER cisternae (Figure 20a - 20c). This group showed elongated microglial cells with electron dense cytoplasm and intracytoplasmic vacuoles with engulfed myelin, characteristic long stretches of endoplasmic reticulum and 1ry lysosomes (Figure 20d). Astrocytes were normal except for scanty vacuolated cytoplasm and disrupted mitochondria (Figure 20e). This group showed intact myelinated axons with smooth regular contour, compact myelin lamellae and intact mitochondria. However, small intra-cytoplasmic vacuoles were noticed (Figure 20f).

Morphometric results:

Were shown in Figure 21.

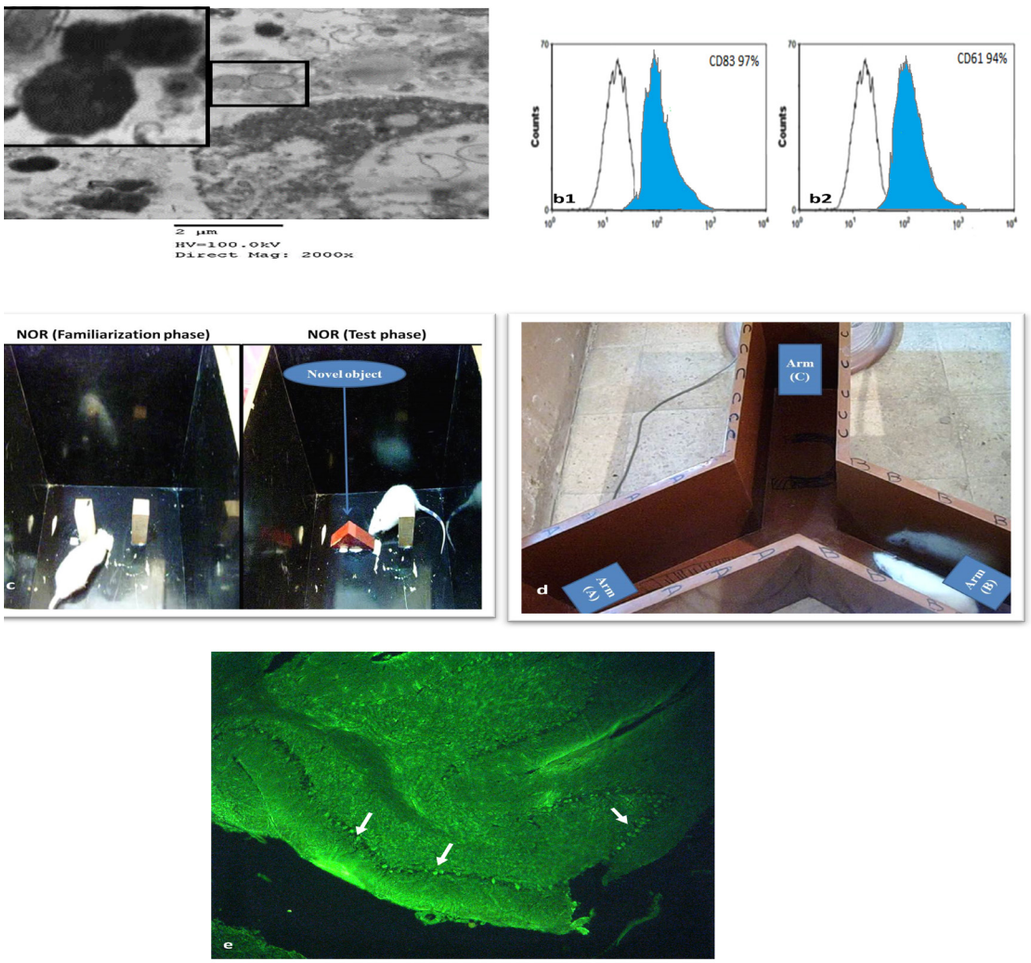

Figure 1: a) Transmission electron microscope characterization of isolated exosomes of cultured MSCs: a) Showing exosomes (scale bar 2µm). Inset showing one exosome (size is less than 70 nm, scale bar 500 nm). b) Fluorescence-Activated Cell Sorting (FACS) isolated exosomes analysis: They express high positivity for CD83 (b1) and CD61 (b2). c) Novel Object Recognition test (NOR) test (Familiarization and Test phase). d) A rat in the arms of Y-maze. e) An image of unstained sections from rat hippocampus of Exo-treated group showing hippocampal homing of the injected PKH26 labeled exosomes after scarifice (arrows). Fluorescent staining X400.

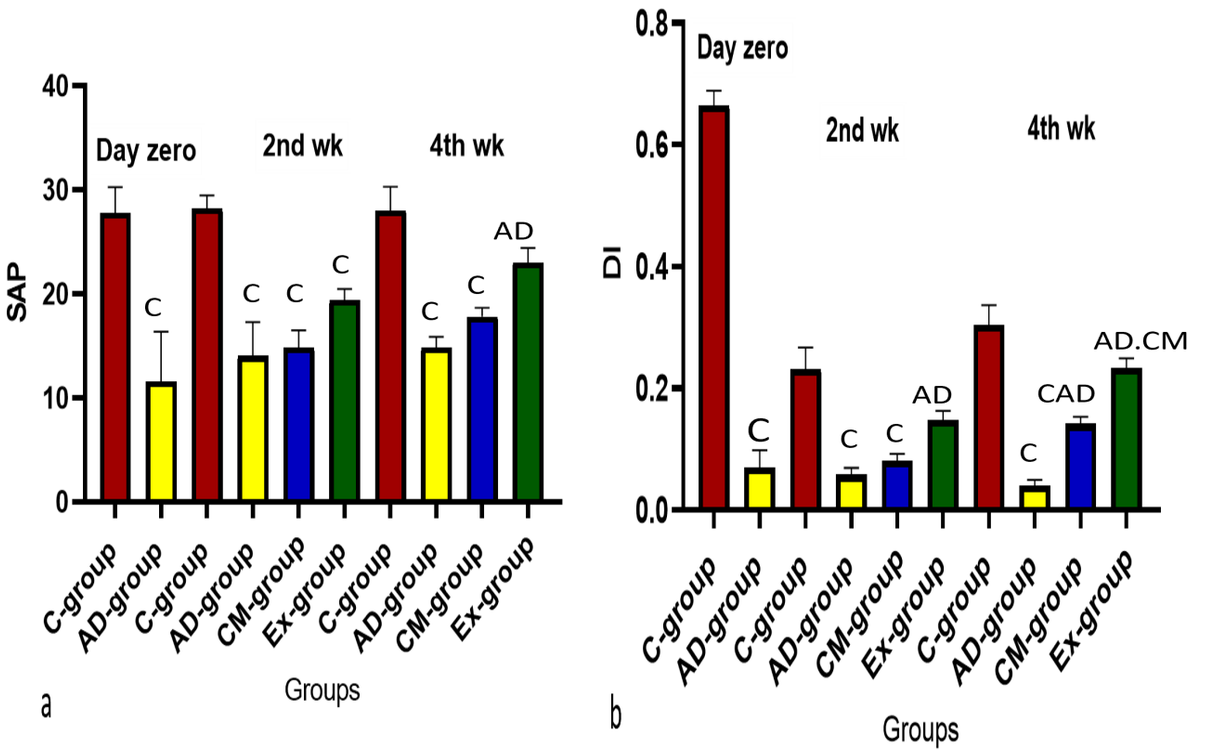

Figure 2: Showing the mean level of: a) Spontaneous alternation behavior percentage (SAP). b) Discrimination index (DI) in all studied groups, (n = 8) C significant versus C-group, AD significant versus AD-group, CM significant versus CM-treated group, at $p < 0.05$.

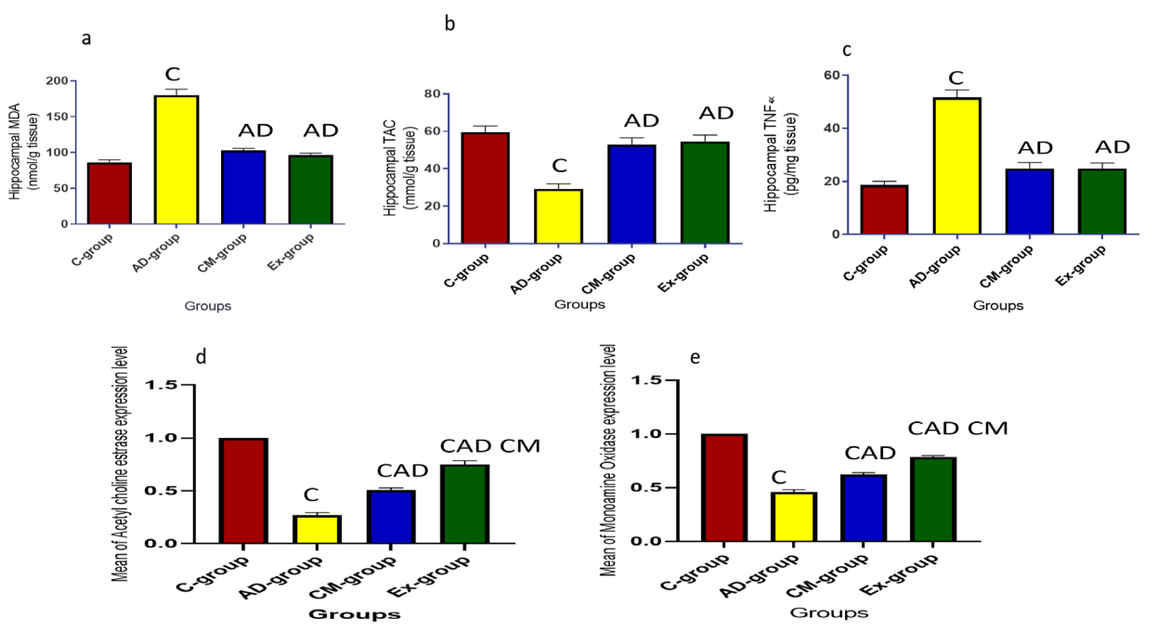

Figure 3: Showing the mean level of hippocampal: a) MDA. b) TAC. c) TNF-α activity. d) AChE expression level. e) MAO expression level in all studied groups (n = 8), C significant versus C- group, AD significant versus AD-group, CM significant versus CM-treated group, at $p < 0.05$.

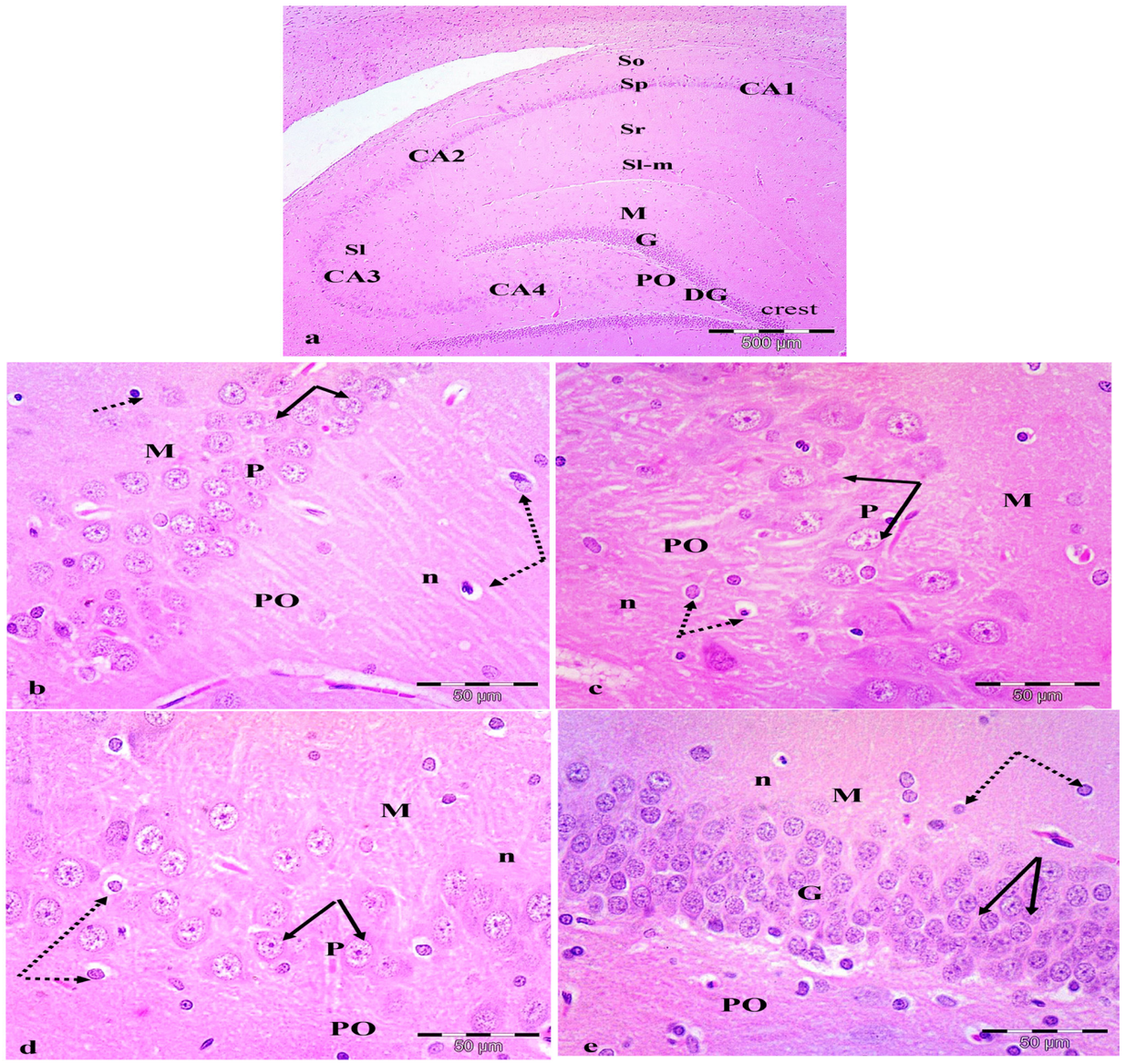

Figure 4: Photomicrographs of sagittal sections of control rat's hippocampi proper and dentate gyrus (DG) showing: a) Hippocampus proper is formed of 4 regions; cornu ammonis (CA); CA1, CA2, CA3 and CA4 areas. Cornu ammonis displays normal laminar organization: stratum oriens (So), stratum pyramidalis (Sp), stratum lucidum (Sl), stratum radiatum (Sr) and stratum lacunosum moleculare (Sl-m). DG is a V-shaped structure, surrounding the CA4 area, with its molecular layer (M), granular cell layer (G) and pleomorphic layer (PO). b) CA1 region; small pyramidal cells have vesicular nuclei with prominent nucleoli (arrows). c and d) CA3 and CA4 regions respectively showing large pyramidal cells (arrows) having nuclei with vesicular appearance and prominent nucleoli. e) The granular cells of DG (arrows) have vesicular nuclei arranged in dense columns. All regions of cornu ammonis are formed of M; superficial molecular layer, P; middle pyramidal layer and PO; deep polymorphic layer. Notice the neuropil (n) and scattered glial cells (dotted arrows). H and E, a X40; b-e X 400.

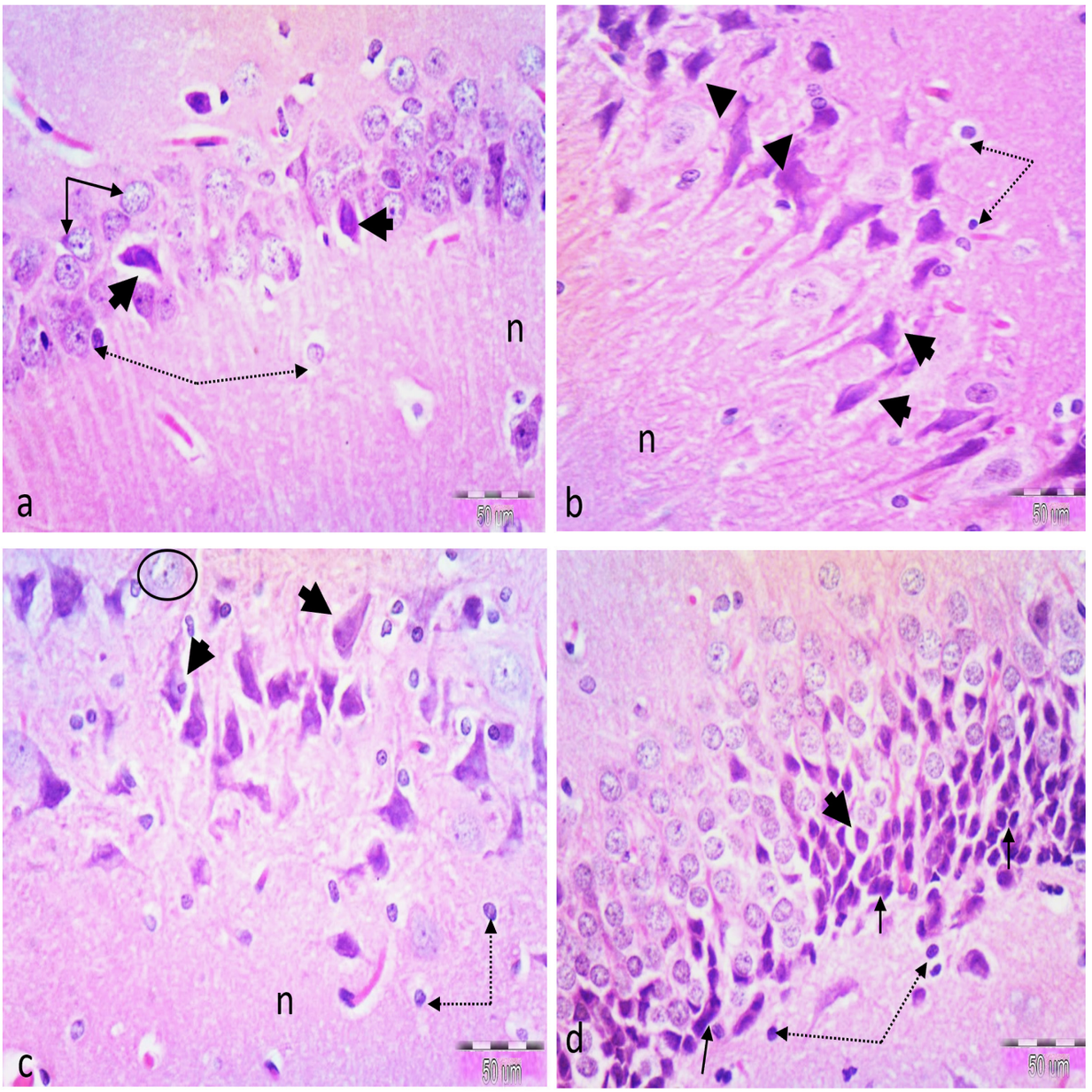

Figure 5: Photomicrographs of the rat hippocampi proper and DG from AD-group showing a) CA1 region with degenerated neurons having shrunken cell bodies and pyknotic nuclei surrounded by perineural space (short arrows). Other neurons have large, rounded central vesicular nuclei (arrows) and basophilic cytoplasm. Notice the congested blood capillaries (c). b and c) CA3 and CA4 regions; most pyramidal cells are shrunken and widely separated, with deeply stained cytoplasm and pyknotic nuclei. Notice the perineural haloes (arrowheads) and degenerated cells with karyolysis (circle). d) DG with shrunken granular cells containing deeply stained cytoplasm and pyknotic nuclei (arrows). Some cells are surrounded by pericellular haloes (arrowhead). Notice the neuropil (n) and scattered glial cells (dotted arrows). H and E X400.

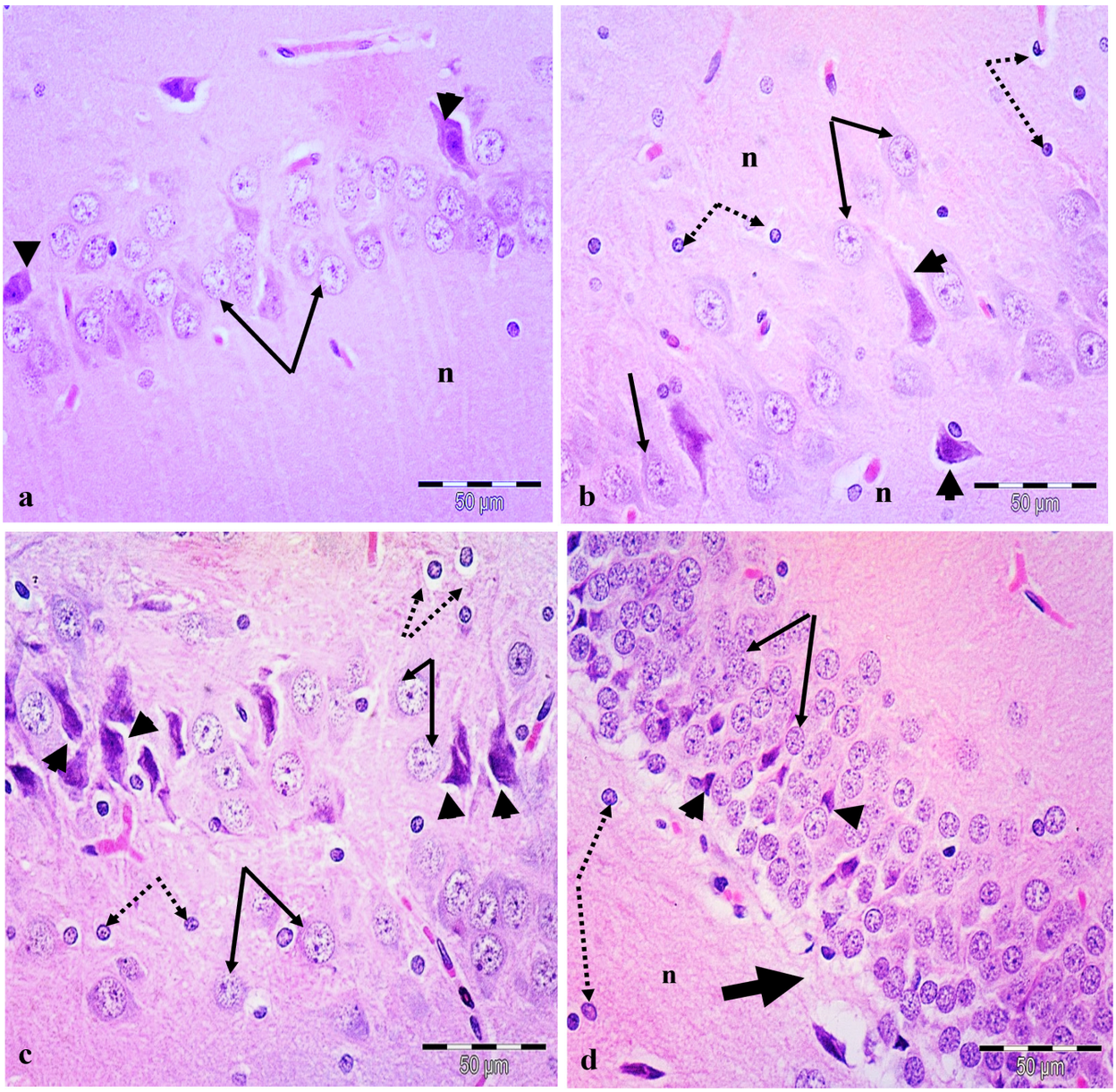

Figure 6: Photomicrographs of the rat's hippocampus proper and DG from CM-treated group: a) CA1 region; most pyramidal neurons appear with basophilic cytoplasm and large central rounded vesicular nuclei (arrows). b& and c) In CA3 and CA4 regions; some pyramidal neurons contain basophilic cytoplasm (arrows). Some shrunken cells with pyknotic nuclei and pericellular halos (short arrows) are seen. d) Most granular cells (arrows) in the DG are normal but, still some cells are shrunken with deeply stained cytoplasm and pyknotic nuclei (short arrows). Vacuolated neuropil is seen in the sub-granular zone (thick arrows). H and E X400.

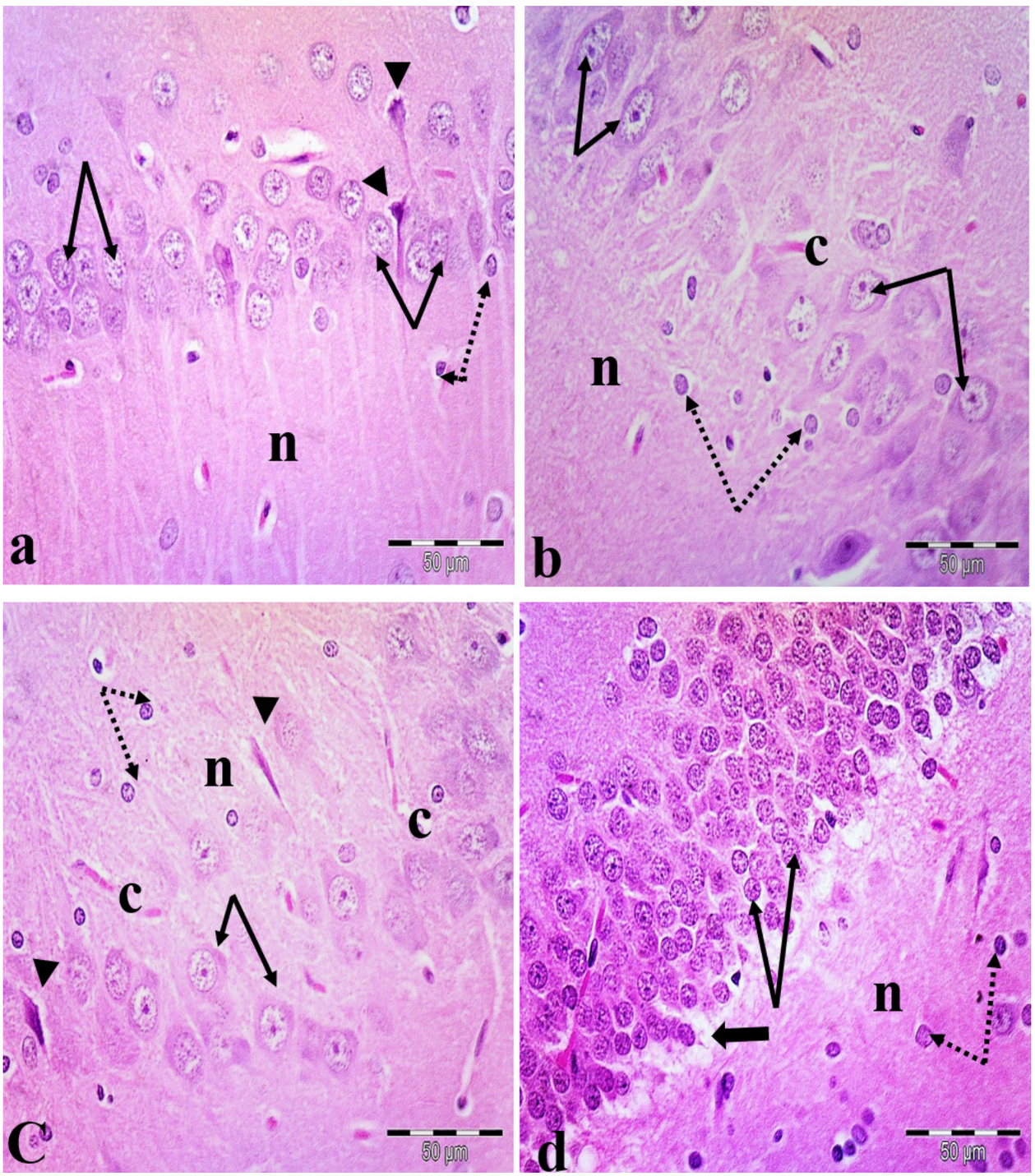

igure 7: Photomicrographs of the rat's hippocampus proper and DG from Exo-treated group: a) CA1 region; most pyramidal neurons appear with basophilic cytoplasm and large central rounded vesicular nuclei (arrows). Notice few shrunken cells with pyknotic nuclei and the pericellular halos (arrow heads). b and c) Most of pyramidal neurons in CA3 and CA4 regions contain vesicular nuclei (arrows) but few shrunken cells with pyknotic nuclei surrounded by pericellular halos. d) In the DG, the granular cell layer preserves most of its normal cells (arrows). Notice slightly vacuolated neuropil in the sub-granular zone (thick arrow). Notice the congested blood capillaries (c) and scattered glial cells (dashed arrows). H and E X400.

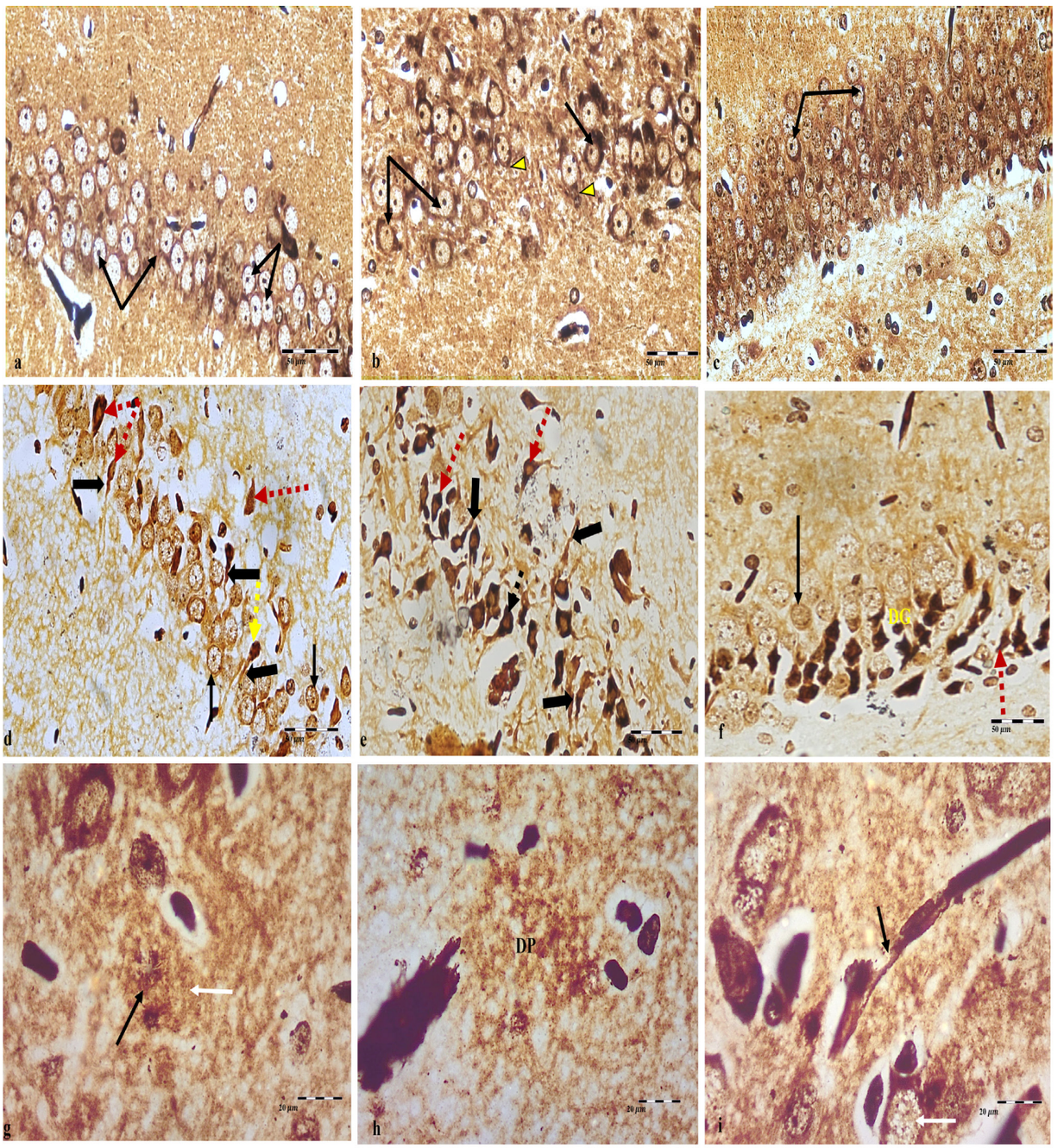

Figure 8: Photomicrographs from rat hippocampus proper and DG showing: a-c) C-group, a) CA1 area contains pyramidal neurons with lightly stained nuclei and prominent nucleoli (arrows). b) CA4 area with pyramidal neurons with lightly stained nuclei and prominent nucleoli (arrows) and faintly stained axons (arrowheads). c) DG with granular neurons with lightly stained nuclei with prominent nucleoli (black arrows). d-i) AD-group, d) CA1 area showing pyramidal neurons with dense intracellular accumulation of NFTs (dotted arrows) obscuring their nuclei and deeply stained degenerated nerve fibers (thick arrows). While other pyramidal neurons appear with lightly stained cytoplasm and prominent nuclei (arrows). e) CA4 area showing numerous pyramidal neurons with dense intracellular accumulation of NFTs (dotted arrows) obscuring their nuclei and the degenerated nerve fibers (thick arrows). f) DG exhibits multiple shrunken degenerated granular neurons with neurofibrillary tangles appear in cytoplasm (dotted arrows) among normal granular neurons with their lightly stained nuclei (arrows). g) Higher magnification of a dense core plaque showing extracellular amyloid deposition (white arrow) with a dense core (black arrow). h) A diffuse plaque (DP) showing extracellular amyloid deposition without core. i) A thinned deeply stained degenerated nerve fiber (black arrow) and neurofibrillary tangles (NFTs) accumulated inside neuronal cell body (white arrow). Silver stain a-f X 400; g-i X 1000.

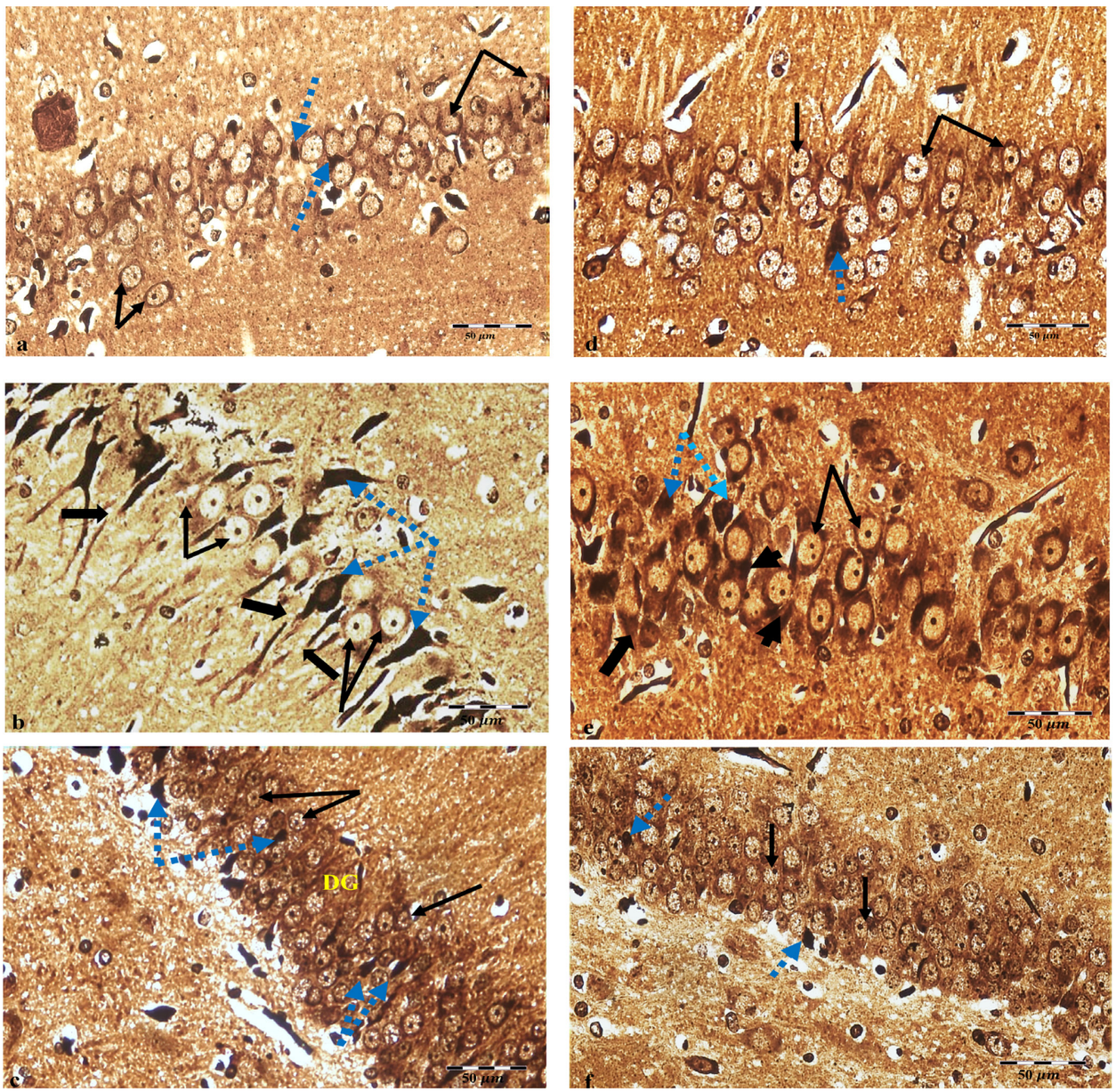

Figure 9: Photomicrographs from rat hippocampus proper and DG showing: a-c) CM-treated group, a) CA1 area showing most pyramidal neurons with lightly stained cytoplasm and prominent nuclei (arrows). While few pyramidal neurons with intracellular accumulation of NFTs (dotted arrows). b) CA4 area still affected; numerous degenerated pyramidal neurons with NFTs (dotted arrows) with deeply stained degenerated and segmented nerve fibers (thick arrows). Others approach normal with lightly stained cytoplasm and prominent nuclei (arrows). c) DG containing preserved most granular neurons (arrows). Still few shrunken degenerated granular neurons with cytoplasmic NFTs (dotted arrows). d-f) Exo-treated group. d-e) CA1 and CA4 areas respectively showing preserved most pyramidal cells (arrows). Notice few pyramidal neurons with NFTs (dotted arrows). In CA4 area, deeply stained degenerated nerve fibers of pyramidal cells (thick arrows). NFTs in the proximal part of some axons (arrow heads). e) DG with preserved most of its granular neurons (arrows). Still few scattered shrunken degenerated granular neurons with cytoplasmic NFTs (dotted arrows). Silver stain X 400

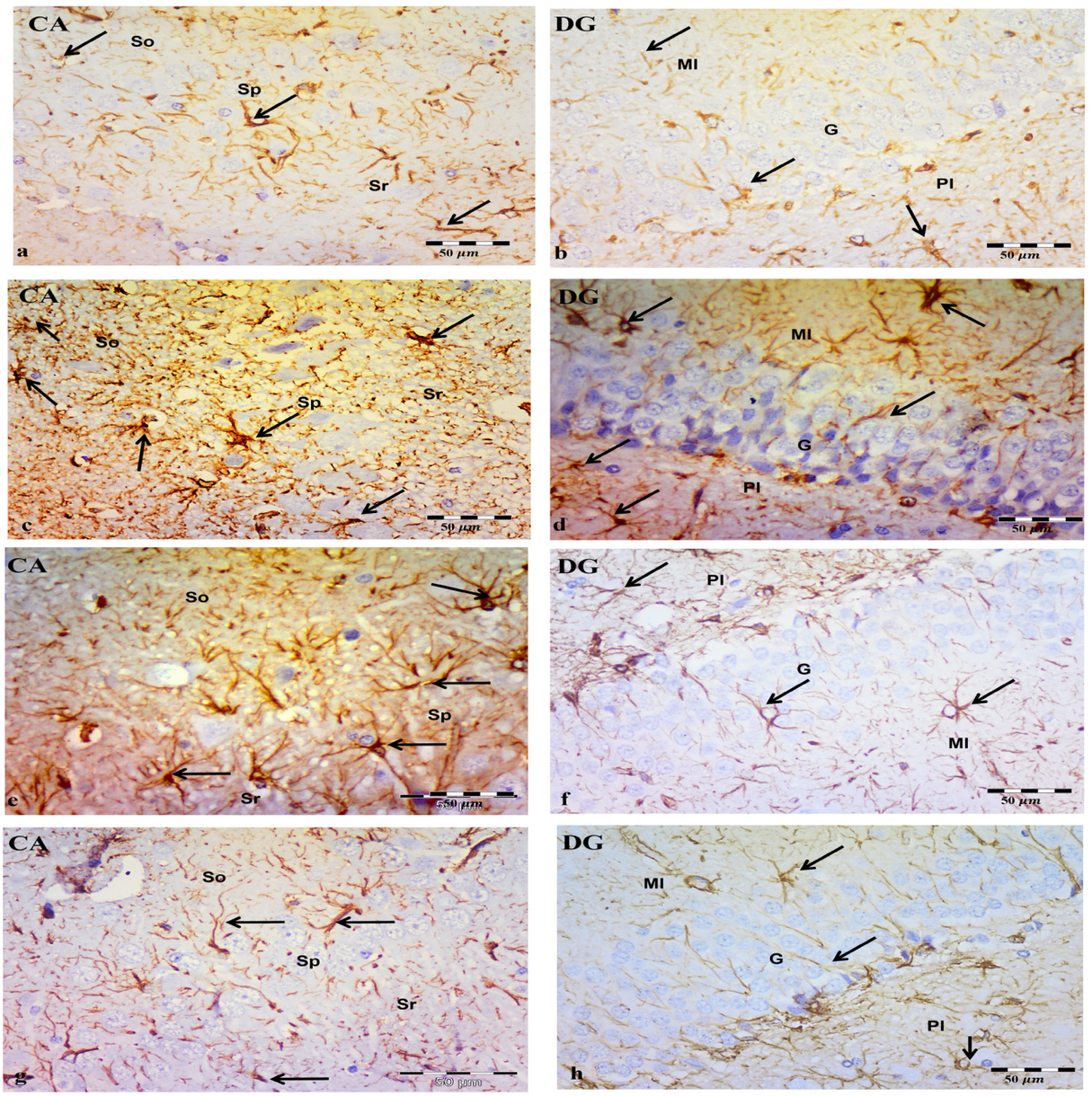

Figure 10: Photomicrographs of sections in the rat 's Cornu ammonis (CA) region: stratum oriens (So), stratum radiatum (Sr) and in between the pyramidal neurons of the stratum pyramidalis (Sp) and DG region; molecular layer (Ml), pleomorphic layer (Pl) and in between the granular cells of the granular cell layer (G). a and b) C group showing few small sized GFAP positive astrocytes with less processes (arrows). c and d) AD-group showing numerous strongly positive GFAP enlarged astrocytes with prominent ramified cytoplasmic processes (arrows). e and f) CM-treated group showing numerous intensely stained GFAP immuno-reactive enlarged astrocytes (arrows) have prominent ramified cytoplasmic processes. g and h) Exo-treated group showing few lightly stained GFAP immuno-reactive astrocytes (arrows). GFAP immuno-staining X400.

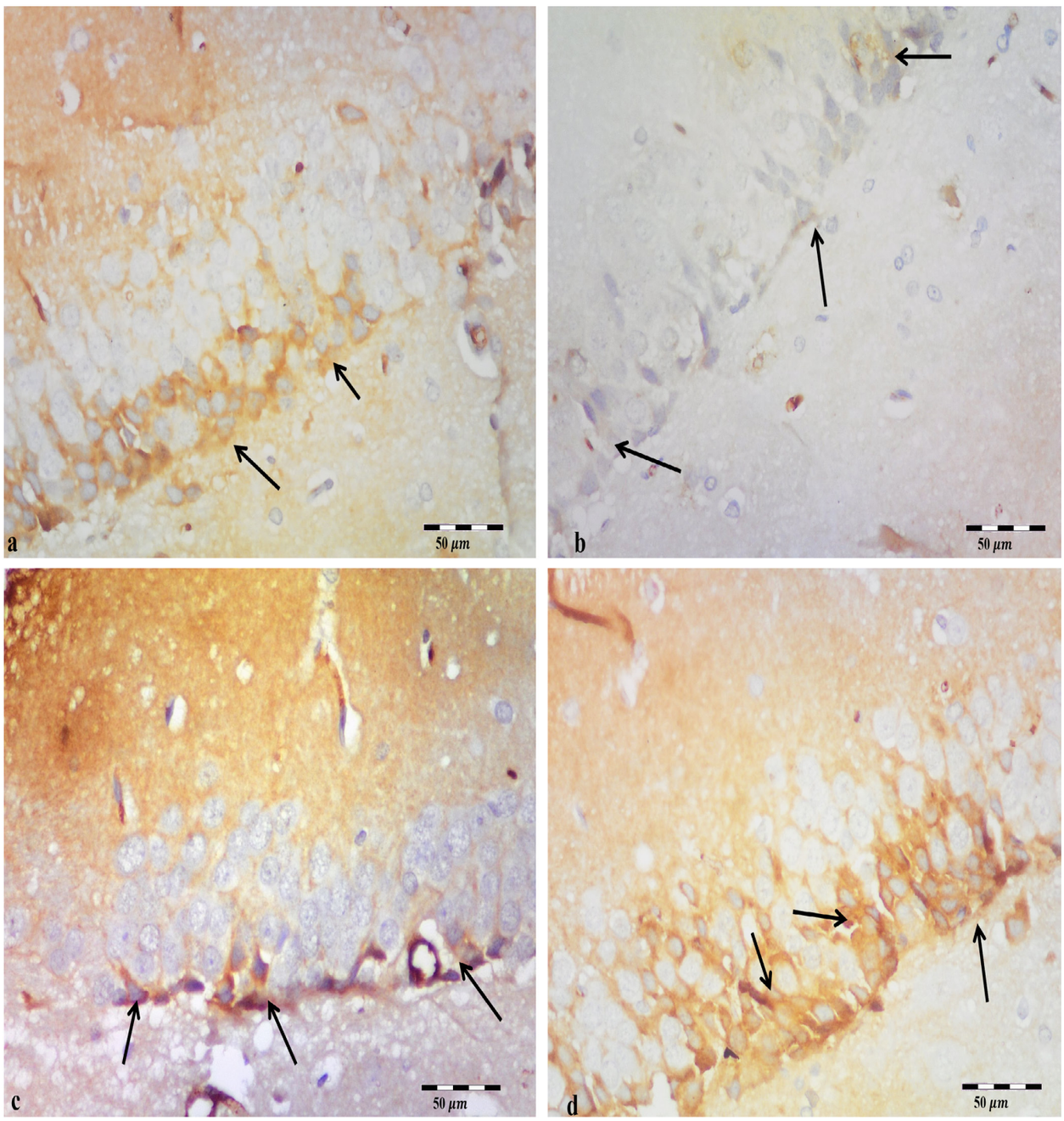

Figure 11: Photomicrographs of anti-nestin immunostaning in the DG among different experimental groups. a) C group showing positive cytoplasmic expression in some granular cells (arrows). b) AD-group showing faint expression in few granular cells (arrows). c) CM-treated group showing apparent increase expression in granular cells (arrows). d) Exo-treated group showing extended nestin immune-positivity in multiple granular cells (arrows). Nestin immuno-staining x 400.

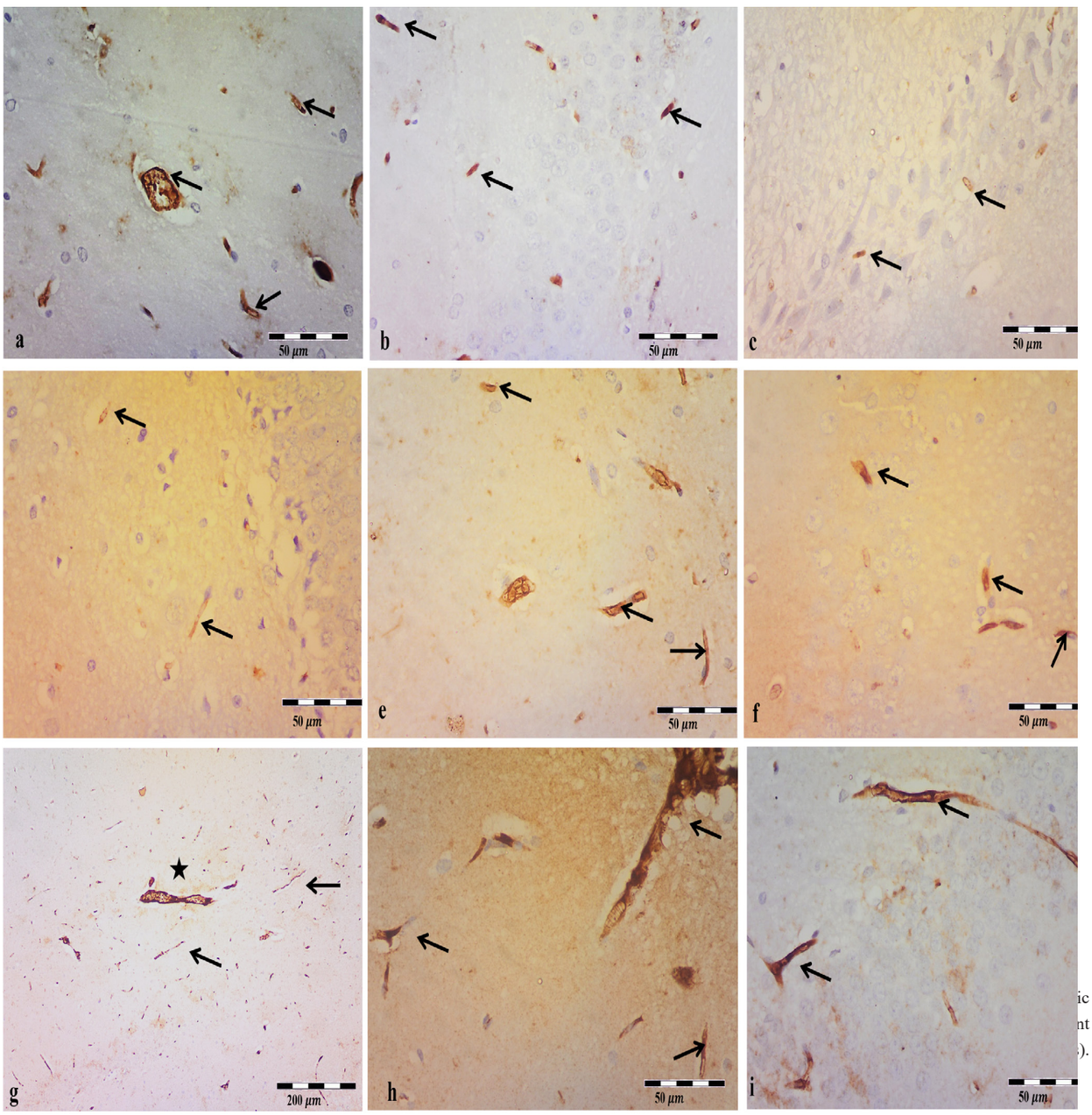

Figure 12: Photomicrographs of microglial anti-CD163 immunostaning in the hippocampus proper and DG. a-b) C group showing positive cytoplasmic expression in some microglia in hippocampus proper (a) and DG (b) (arrows). c-d) AD group showing decreased positive microglia with faint expression in hippocampus proper (c) and DG (d) (arrows). e-f) CM-treated group showing positive cytoplasmic staining in some microglia in hippocampus proper (e) and DG (f) (arrows). g,h,i) Exo-treated group showing: g) Immune-reactive microglia in close proximity to blood capillary (star). h,i) strong positive cytoplasmic expression in numerous microglia in hippocampus proper (h) and DG (i) (arrows). Anti-CD163 immuno-staining x 400 (except g x 100).

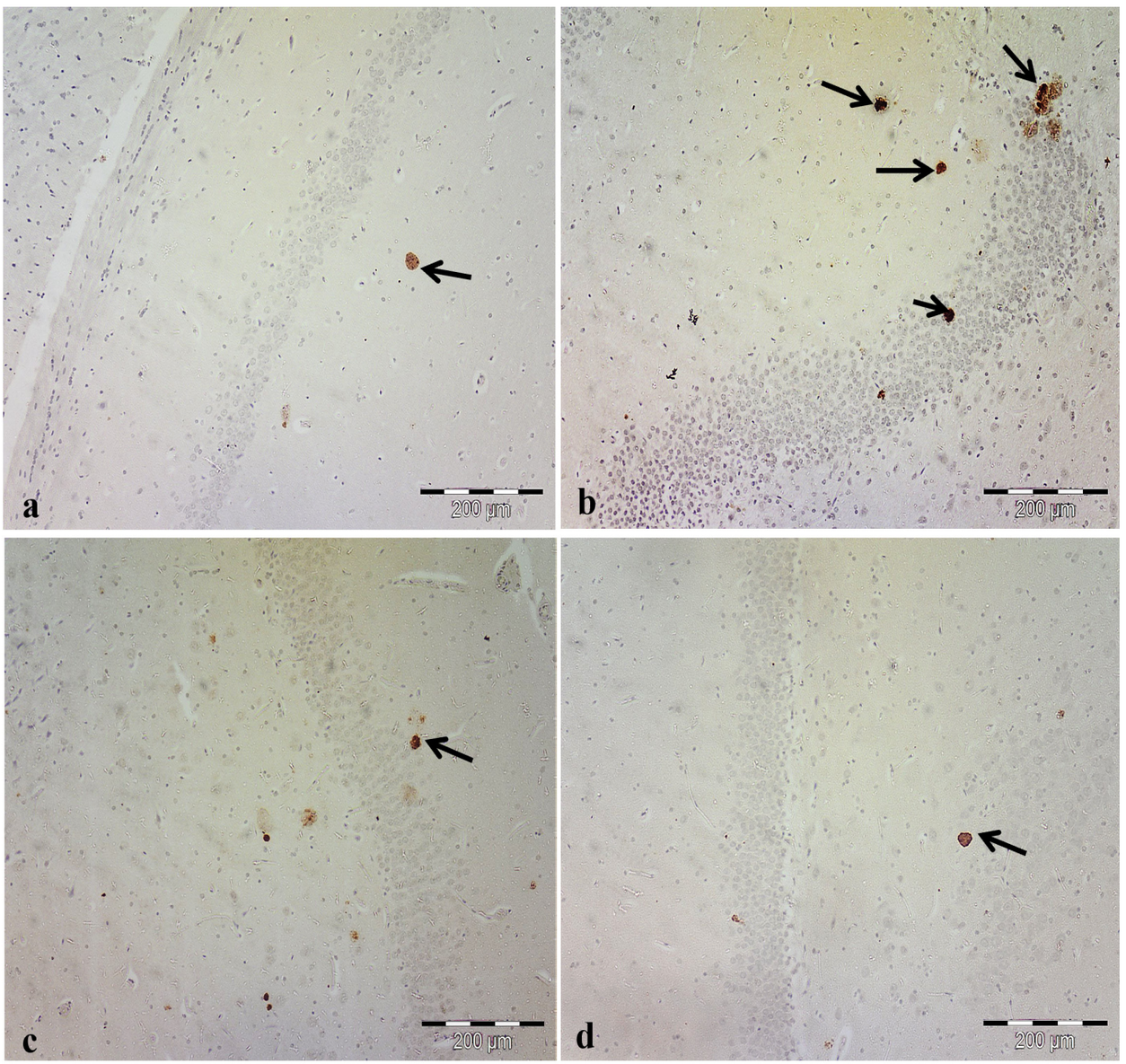

Figure 13: Photomicrographs of microglial anti-CD86 immunostaning in the hippocampus proper and DG from: a) C group showing positive cytoplasmic staining in few scattered glial cells (arrows). b) AD group showing increased immune-positive microglial cells (arrows). c) CM-treated group showing positive cytoplasmic expression in some microglial cells (arrows). d) Exo-treated group showing positive cytoplasmic expression in scattered microglial cells (arrows). Anti-CD86 immuno-staining x 100.

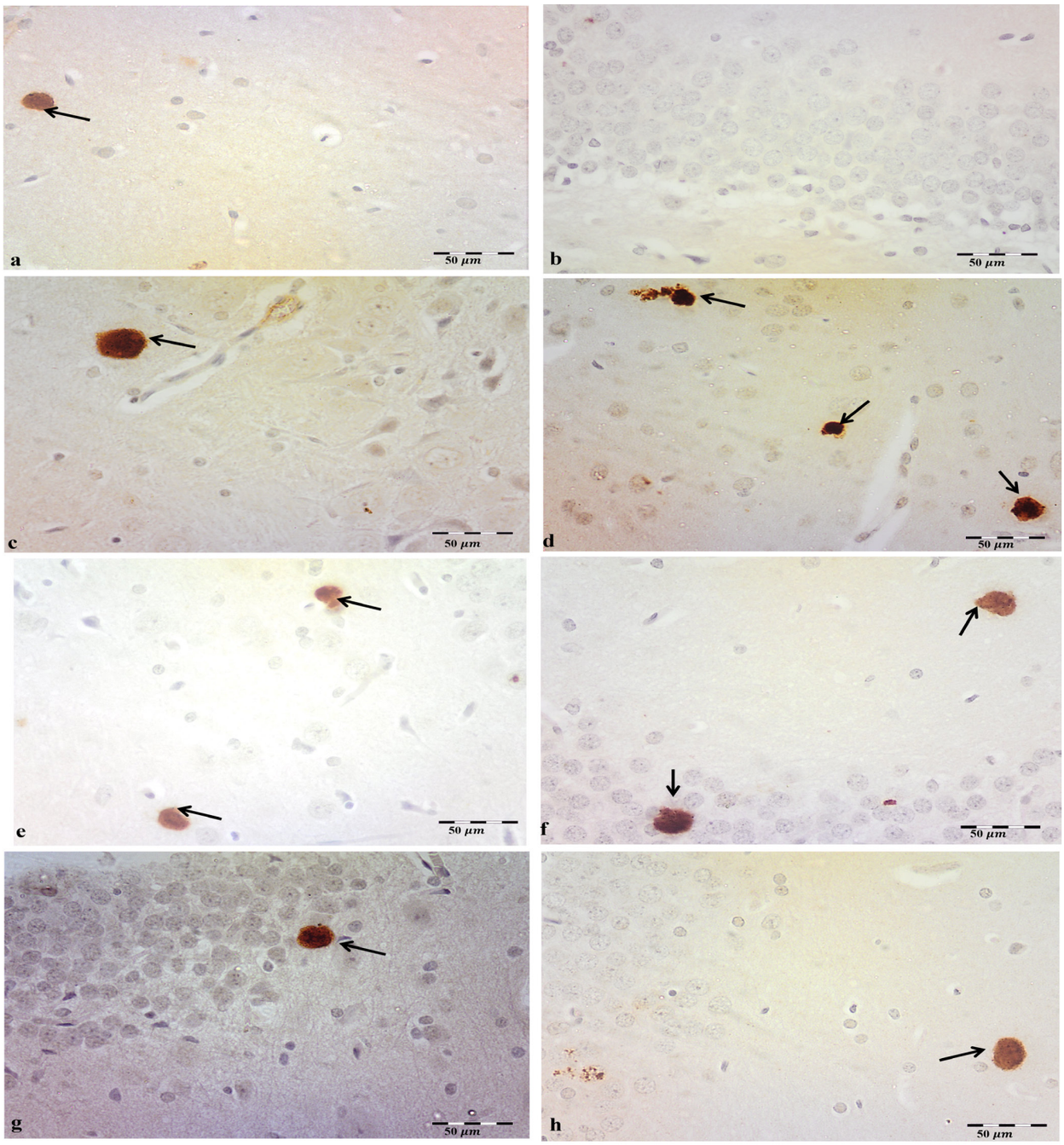

Figure 14: Photomicrographs of microglial anti-CD86 immunostaning in the hippocampus proper and DG from: a, b) C group showing positive cytoplasmic staining in few scattered glial cells (arrows). c, d) AD group showing increased immune-positive microglial cells (arrows). e, f) CM-treated group showing positive cytoplasmic expression in some microglial cells (arrows). g, h) Exo-treated group showing positive cytoplasmic expression in scattered microglial cells (arrows). Anti-CD86 immuno-staining x 400.

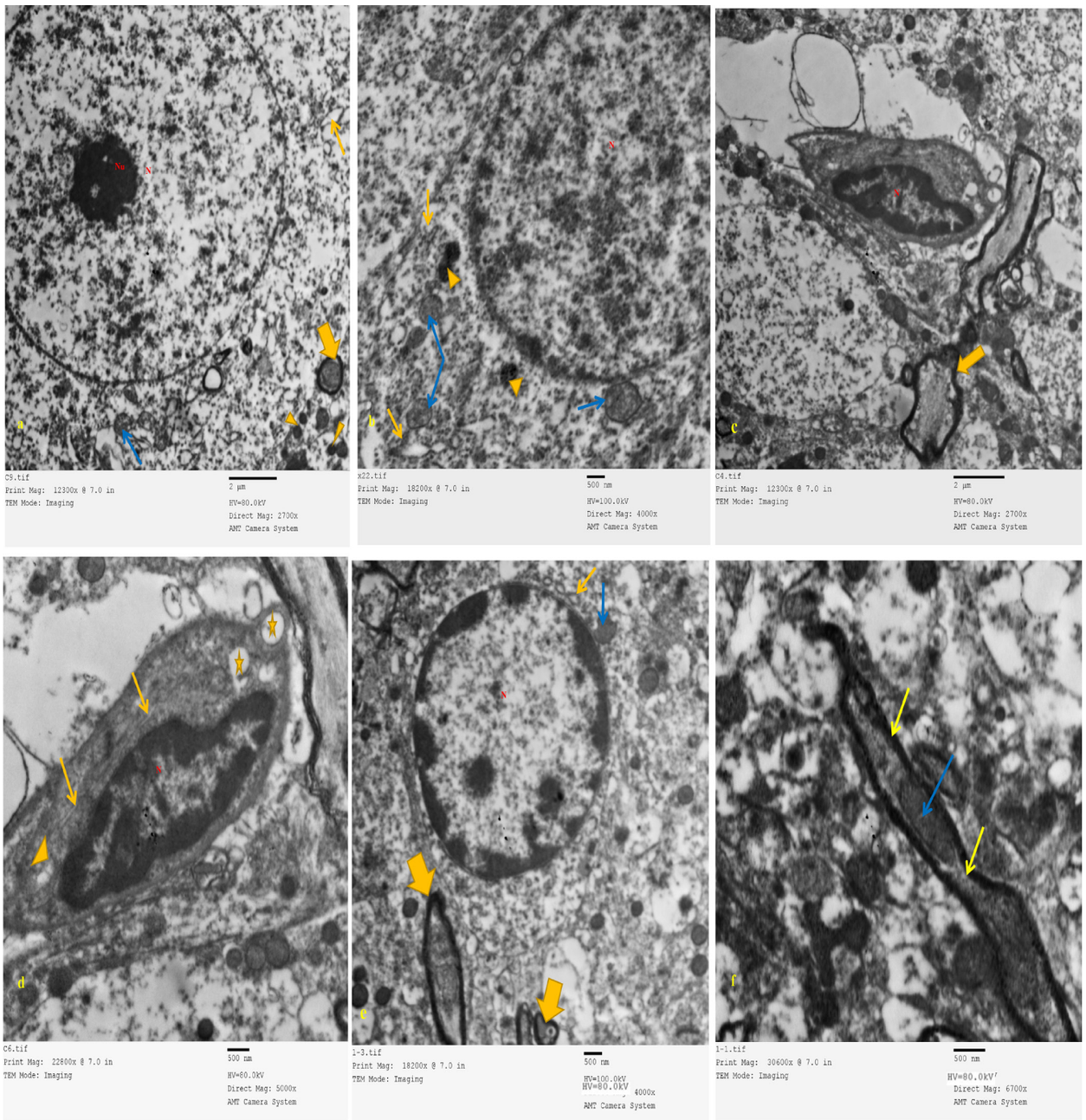

Figure 15: Electron-micrographs of rat hippocampus from C-group showing: a) A pyramidal neuron with large vesicular central nucleus (N) with dispersed chromatin and prominent nucleolus (Nu), the abundant rER (yellow arrow), intact mitochondria (blue arrow) and1ry lysosomes (arrowheads). Notice intact myelinated axons (thick arrows). b) Higher magnification of a pyramidal neuron showing abundant rER (yellow arrows), intact mitochondria (blue arrows) and 2ry lysosomes (arrowheads). c) A microglial cell with an elongated nucleus (N) and peripheral heterochromatin. Notice myelinated axons (arrows). d) Higher magnification showing distinctive long stretches of endoplasmic reticulum (yellow arrows), electron dense bodies (arrowhead) and cytoplasmic vacuoles (stars). e) An astrocyte having a nucleus (N) with darkly condensed chromatin and surrounded by little cytoplasm containing organelles; mitochondria (blue arrow) and rER (yellow arrow). Notice myelinated axons (thick arrows). f) Myelinated axon with regular smooth contour and compact myelin lamellae (black arrows). Notice the intact mitochondria (blue arrow) in the axoplasm.a, c, e x 2700, bx4000, Dx 5000, Fx 6700.

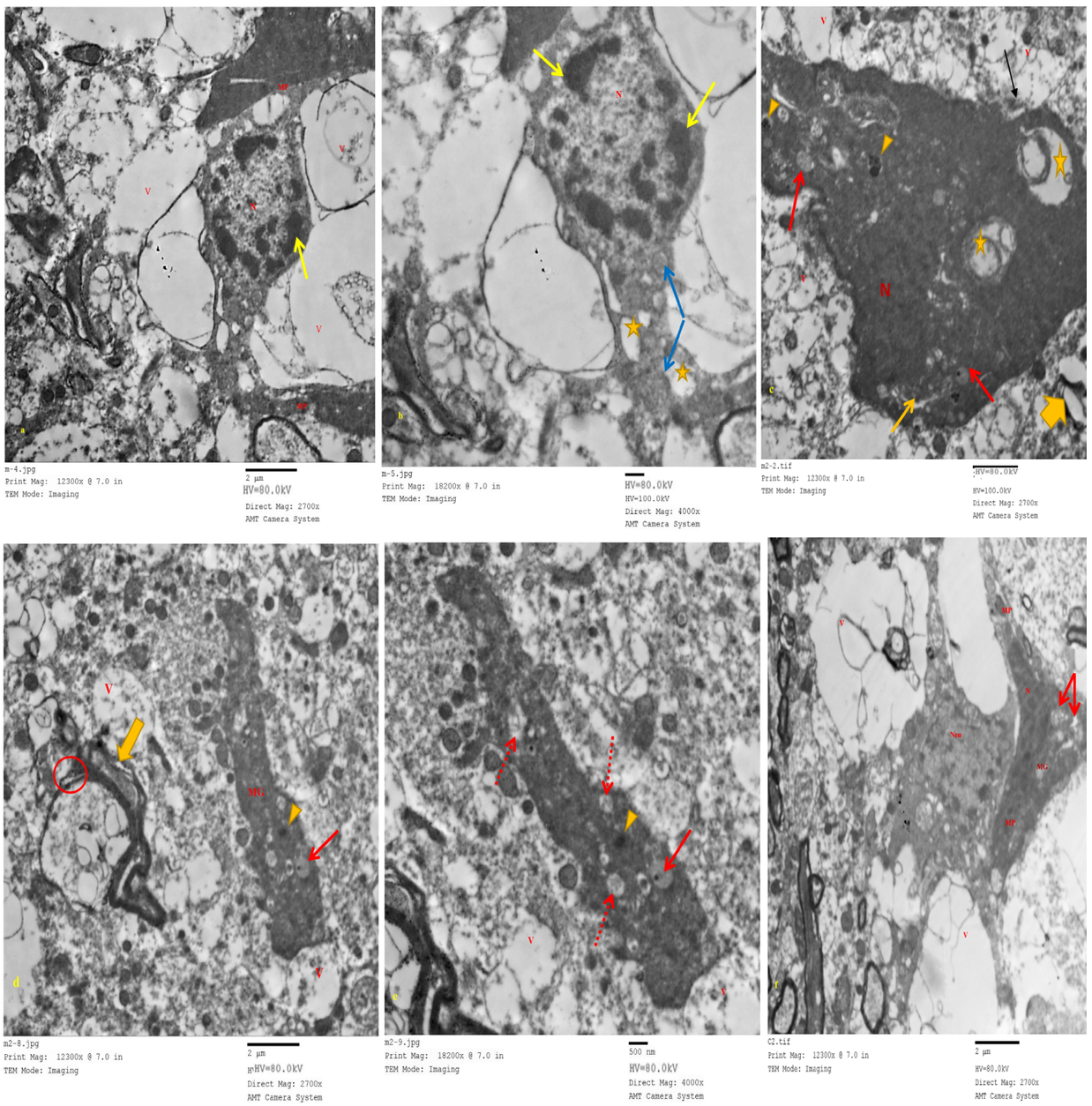

Figure 16: Electron-micrographs of rat hippocampus from AD-group showing a) Damaged shrunken neuron with scanty cytoplasm and condensed peripheral chromatin (black arrow). Notice microglial processes surrounding the damaged neuron (MP) and the vacuolated areas surrounding neuropil (V). b) Higher magnification revealed the condensed peripheral nuclear chromatin (black arrows) intracytoplasmic vacuolations (stars) and loss of cytoplasmic organelles except of some mitochondria (blue arrows). c: A neuron with electron dense cytoplasm and dark heterochromatic eccentric nucleus (N) surrounded by vacuolated neuropil (V) with notched plasma lemma (black arrows). Notice the 1ry lysosome (red arrows), 2ry lysosomes (arrowheads), dilated cisternae of rER (yellow arrow), intracytoplasmic vacuolations with myelin-like figures (stars) and decompacted myelinated axons (thick arrow). d) Dark elongated microglial cell (MG) with electron dense cytoplasm with 1ry lysosome (red arrow) and 2ry lysosome (arrowhead). Notice irregular decompacted myelinated axon (thick yellow arrow) with areas of focal interruption of myelin (circle) and vacuolated neuropil (V). e) Higher magnification revealed 1ry lysosome (red arrow) and 2ry lysosome (arrowhead) and multiple intracytoplasmic vacuoles (dotted arrows). f) A dark microglial cell (MG) with electron dense cytoplasm, dark heterochromatic nucleus (N) and intracytoplasmic vacuolations (arrows) with its processes (MP) surrounding damaged shrunken neuron (Neu). Notice the vacuolated neuropil (V). a, c, d,f X2700, b ,eX4000.

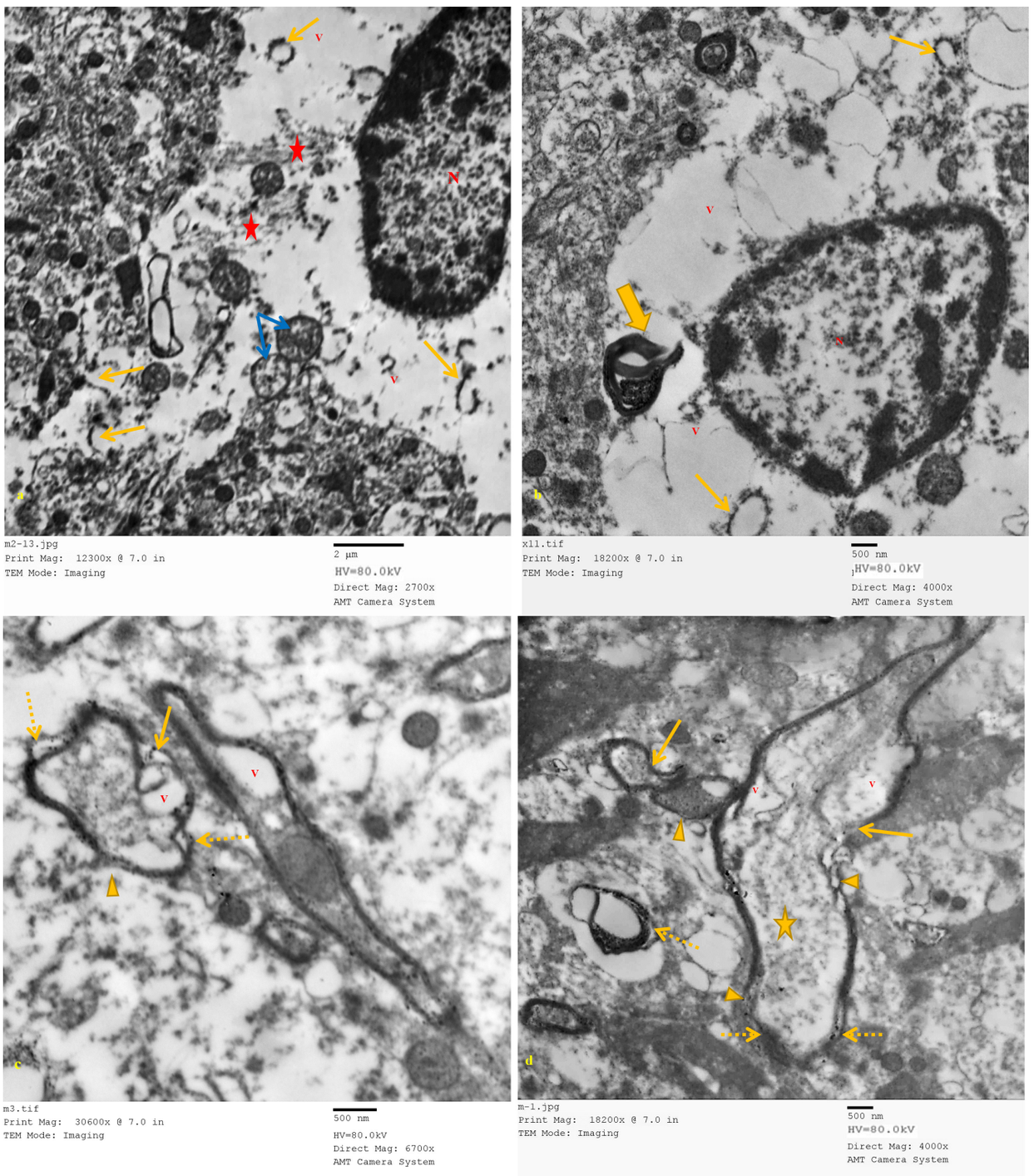

Figure 17: Electron-micrographs of rat hippocampus from AD-group showing: a) An astrocyte with cytoplasmic vacuolation (V), irregular nucleus with little peripheral electron dense nuclear chromatin (N), remnants of rER (yellow arrows), remnants of microfilaments (red stars) and damaged mitochondria with disrupted cristae (blue arrows). b) Higher magnification of an astrocyte with cytoplasmic vacuolations (V), irregular nucleus with little peripheral electron dense nuclear chromatin (N) and intra-cytoplasmic engulfed myelin (thick arrow). Notice the dilated cisternae of rER (yellow arrows). c, d) Degenerated myelinated axons with irregular outlines, large axoplasmic vacuoles (V), areas of thinning (arrows) and areas of focal interruption (arrowheads) of myelin sheath with decompaction (dotted arrows) of myelin lamellae and disruption of neurofilaments (star). aX2700, b, dX4000, c X6700.

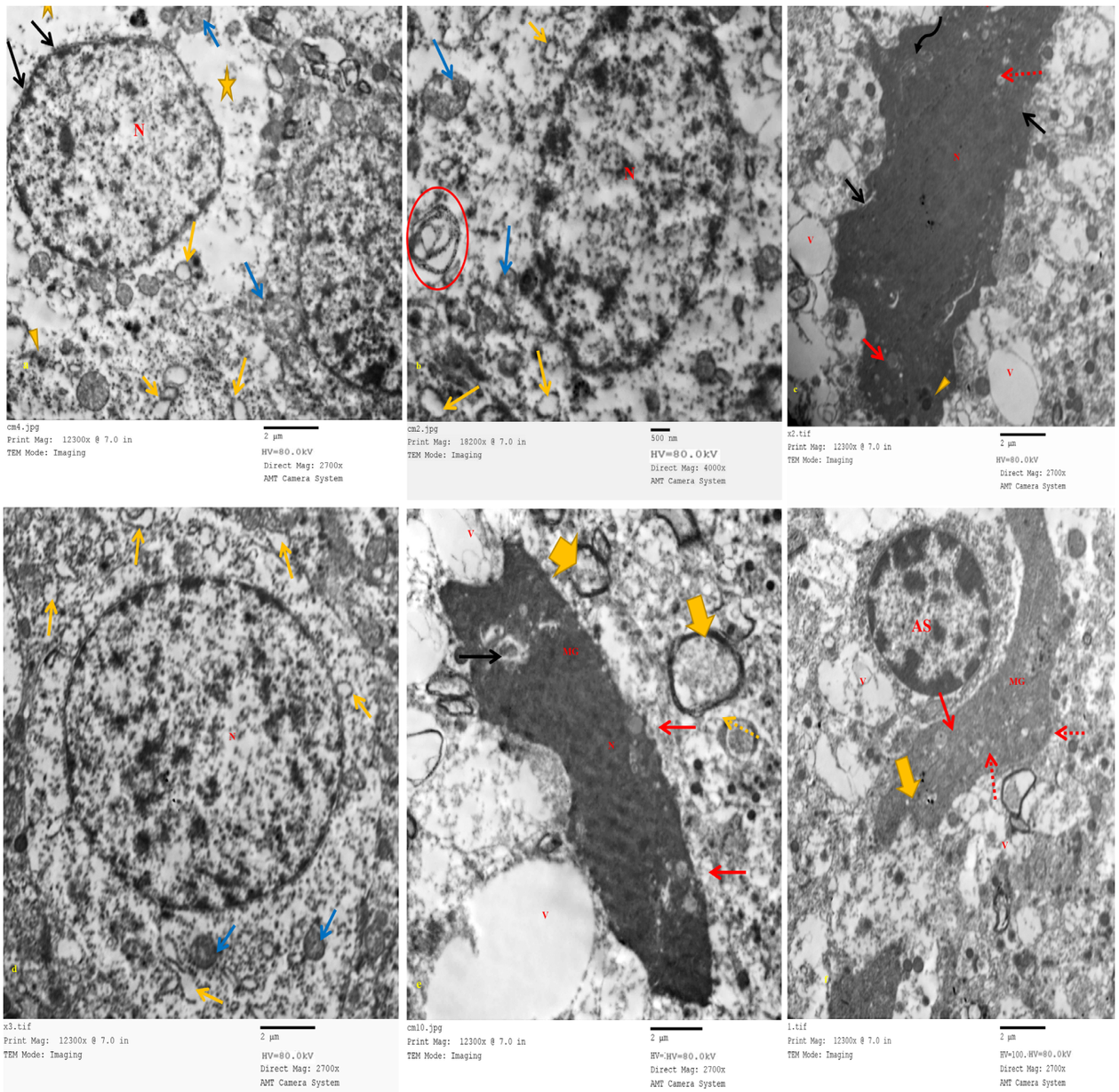

Figure 18: Electron-micrographs of rat hippocampus from CM-group showing a) A neuron with areas of empty cytoplasm (star) and euchromatic nucleus (N) with areas of increased peripheral chromatin density (black arrows). Notice the dilated cisternae of rER (yellow arrows), 2ry lysosome (arrowheads), some damaged mitochondria with disrupted cristae (blue arrows). b) Higher magnification of a neuron showing euchromatic nucleus (N), dilated cisternae of rER (yellow arrows), some damaged mitochondria with disrupted cristae (blue arrows) and myelin-like figure (circle). c)A neuron with electron dense cytoplasm and dark heterochromatic nucleus (N) surrounded by vacuolated neuropil (V). Notice its notched plasma lemma (black arrows), 1ry lysosomes (red arrows), 2ry lysosome (arrowhead), intracytoplasmic vacuolations (dotted arrows) and myelin-like figure (curved arrow). d)A neuron with vesicular nucleus (N) and dispersed chromatin. Notice the dilated cisternae of rER (yellow arrows) and the apparently intact mitochondria (blue arrows). e) A dark elongated microglial cell (MG) with dark heterochromatic nucleus (N), electron dense cytoplasm, 1ry lysosomes (red arrows) and intracytoplasmic vacuole with engulfed myelin (black arrow). Notice the decompacted myelinated axons (dotted arrows) with interruption of myelin sheath (thick arrow) and vacuolated neuropil (V). f) An elongated microglial cell (MG) with cytoplasmic processes (thick arrow) and electron dense cytoplasm with multiple intracytoplasmic vacuoles (dotted arrows) and 1ry lysosomes (red arrow). Notice damaged astrocyte (AS) with scanty cytoplasm and vacuolated neuropil (V). a,c,d ,e,fX 2700, bX 4000.

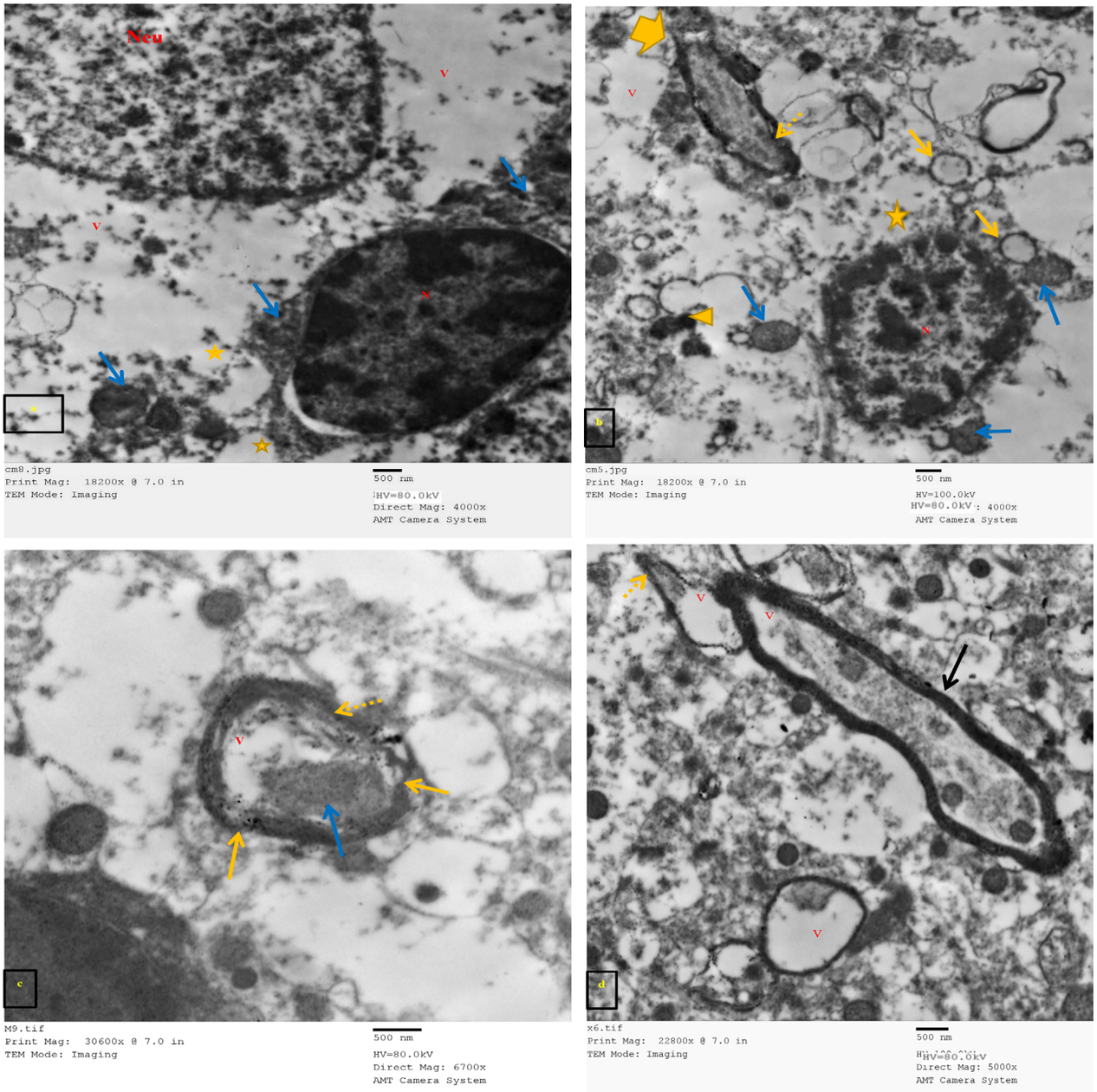

Figure 19: Electron -micrographs of rat hippocampus from CM-group showing: a) An astrocyte showing nucleus with electron dense nuclear chromatin (N), areas of empty cytoplasm (stars) and damaged mitochondria with disrupted cristae (blue arrows). Notice damaged neuron (Neu) with vacuolated cytoplasm (V) in close proximity to astrocyte. b) An astrocyte with areas of empty cytoplasm (star), nucleus with electron dense nuclear chromatin (N), dilated cisternae of rER (yellow arrows), 2ry lysosome (arrowhead) and intact mitochondria (blue arrows). Notice degenerated myelinated axon with focal interruption of myelin (thick arrow), areas of thinning (dotted arrow) and vacuolated neuropil (V). c)Degenerated myelinated axon with irregular outlines; areas of thinning (yellow arrows) and areas of decompaction of myelin lamellae (dotted arrow) with large axoplasmic vacuole (V) and shrunken disrupted mitochondria (blue arrow). d) Degenerated myelinated axons with irregular outlines (dotted arrow) and large axoplasmic vacuole (V). Notice a myelinated axon with compact myelin lamellae (black arrow) with small axoplasmic vacuole (V). a, b X 4000, c X6700, d X5000.

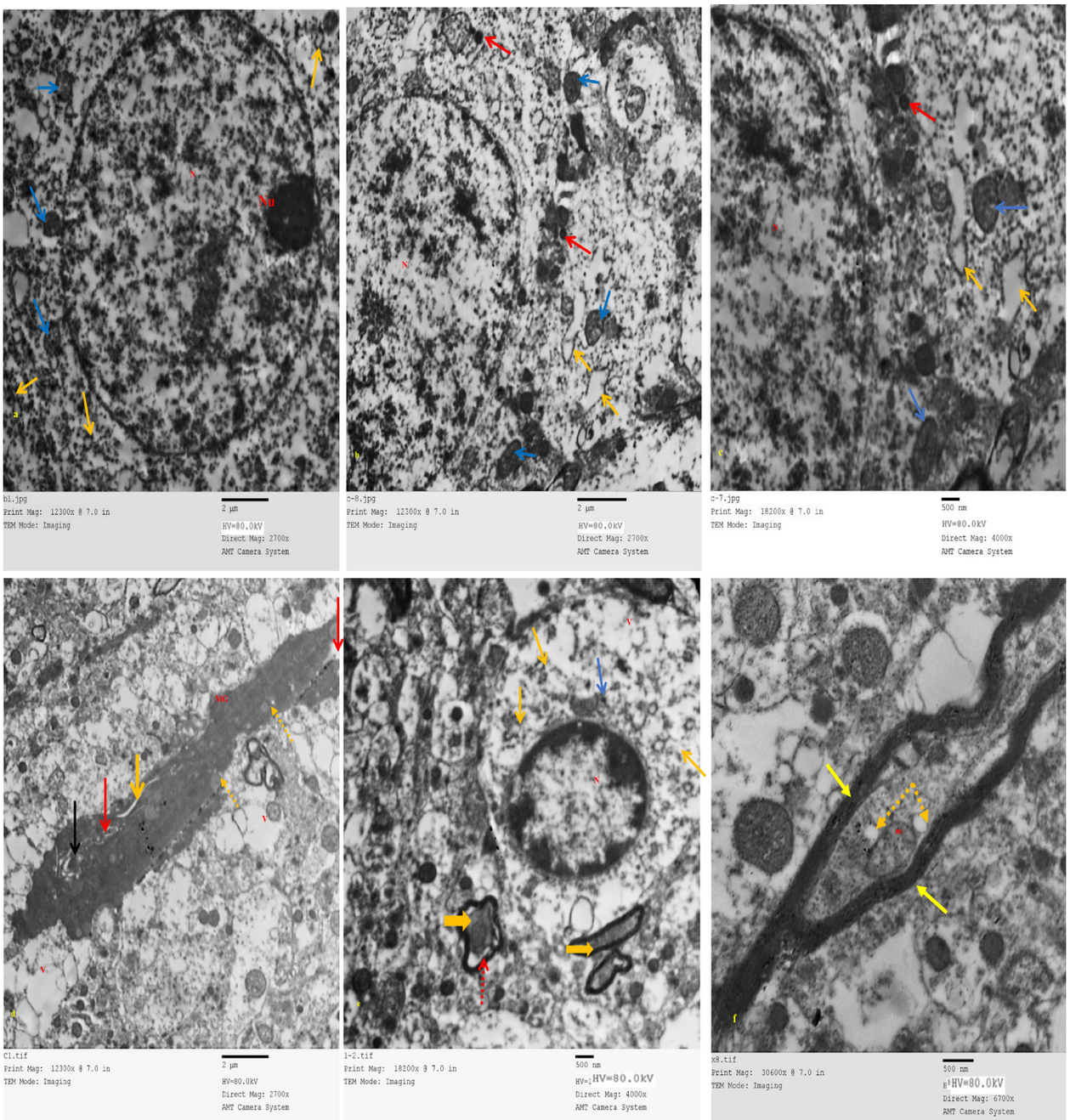

Figure 20: Electron -micrographs of rat's hippocampus from Ex-group showing a) A neuron with vesicular nucleus (N) with dispersed chromatin and prominent nucleolus (Nu). Notice intact mitochondria (blue arrows) and dilated cisternae of rER (yellow arrows). b) A neuron with vesicular nucleus (N) with dispersed chromatin. c) Higher magnification showing intact mitochondria (blue arrows), dilated cisternae of rER (yellow arrows) and 1ry lysosomes (red arrows). d)An elongated microglial cell (MG) with electron dense cytoplasm and intracytoplasmic vacuoles (red arrow) with engulfed myelin (black arrow), long stretches of endoplasmic reticulum (yellow arrow) and 1ry lysosomes (dotted arrow). Notice the vacuolated neuropil (V). e) An astrocyte having nucleus (N) with densely packed chromatin and surrounded by scanty vacuolated cytoplasm (V), disrupted mitochondria (blue arrow) and intact rER (thin yellow arrows). Notice myelinated axons with compact myelin lamellae (thick arrows) and little axoplasmic vacuolations (dotted arrow). f) Myelinated axon with a regular smooth contour and compact myelin lamellae (black arrows). The axoplasm containing intact mitochondria (m) and small vacuoles (dotted arrow). A,b,c X 2700, d,f X 400, fX6700.

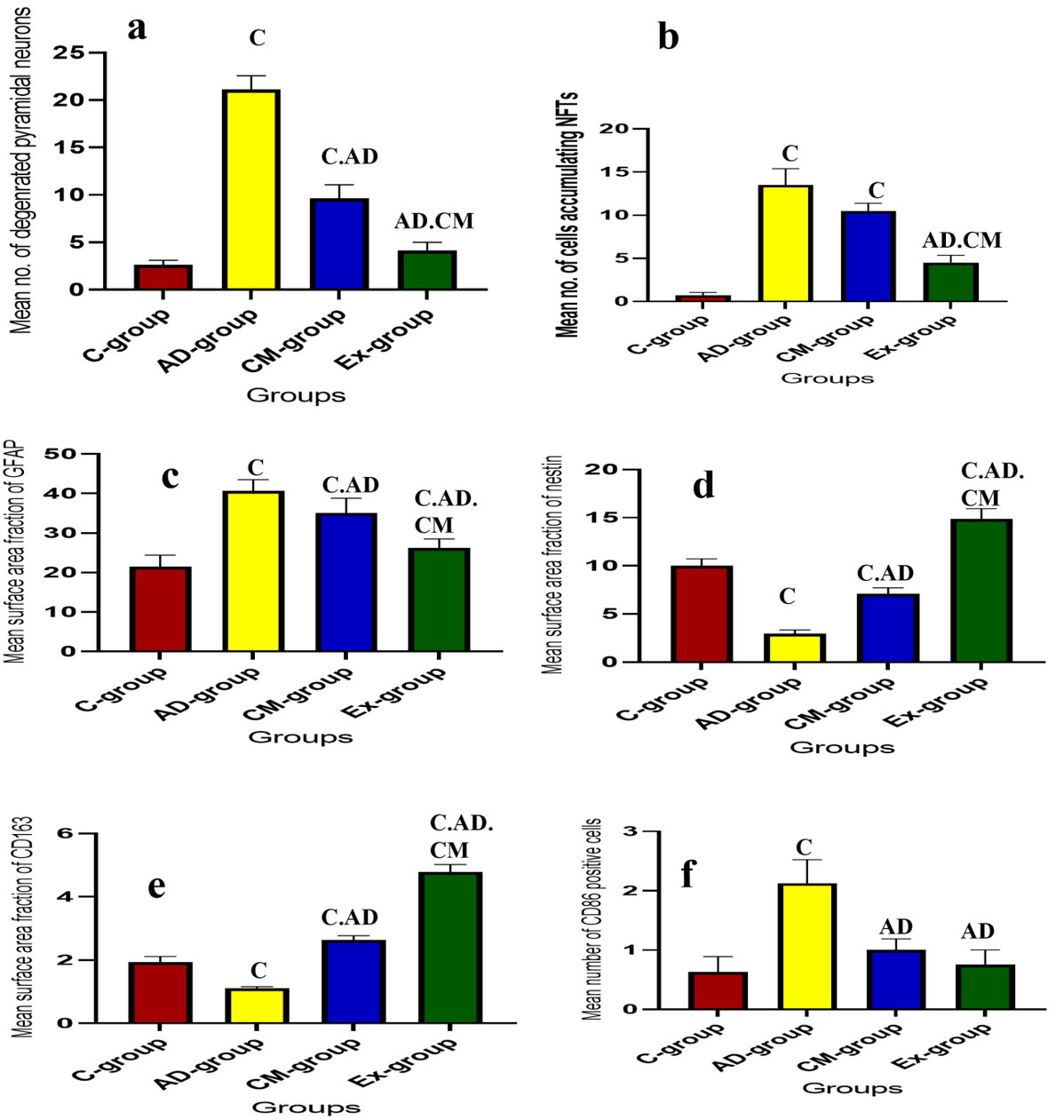

Figure 21: Showing the mean number in all studied groups of a) Degenerated pyramidal neurons. b) The cells accumulating neurofibrillary tangles (NFTs). c) Surface area fraction of GFAP expression. d) Surface area fraction of nestin expression. e) Surface area fraction of CD-163 expression. f) CD-86 positive cells. (n = 8) C significant versus C-group, AD significant versus AD-group, CM significant versus CM-treated group, at $p < 0.05$.

DISCUSSION

The most common cause of dementia is Alzheimer's disease (AD), which impacts about 47 million people worldwide and estimated to triple by 2050 to triple by 2050[31]. Studies showed that aluminum (Al) is associated with several neurophysiologic processes that are responsible for the characteristic structural alterations of AD. It is a heavy metal that has rapid accessibility to our body through antacids, tools, water and additives. It easily accesses the blood-brain barrier (BBB) and precipitates in the brain. Excessive accumulation of beta-amyloid (Aβ) leads to the creation of amyloid plaques (APs), causing neurotoxicity in both people and animals. Rats with Alzheimer-like disease produced by AlCl3 are found to be the most widely used animal model that mimics human AD[32].

With high clinical interest in regenerative medicine, Mesenchymal Stem/Stromal Cells have been widely studied due to their multipotency, wide distribution and relative ease of isolation and expansion in vitro. Stem cells (MSCs) release paracrine factors that influence tissue repair and regeneration and are most likely responsible for the main beneficial effects of stem cells[32]. Moreover, studies suggested that the paracrine actions of MSCs are mediated by extracellular vehicles (EVs), specifically exosomes. Hence, this study was conducted to investigate the therapeutic effects of conditioned media and exosomes.

Cognitive deficits were considered an essential clinical indicator and a serious health-related concern in AD[33]. In the current study, AD rat model revealed behavioral changes including a decline in learning and working memory, as well as spatial and recognition memory, as measured by the open field test, Y-maze and novel object recognition (NOR) tests. Regarding the open field test, the AD group showed anxiety-like behaviors and a substantial drop in locomotor activity compared to the C group. The Y-maze and NOR tests in the AD group revealed a significant drop in discrimination index (DI) and spontaneous alternation behavior percentage (SAP) it was in line with a previous study[34] which detected alternation in open field test in rat AD.

Chronic inflammatory disorders are exacerbated by oxidative stress as it induces damage, such as oxidized proteins and lipid peroxidation, leads to neurodegeneration, which is frequently observed in brain disorders[35]. Aluminum accesses the BBB and accumulates in many brain parts. Additionally, it induces formation of the free radicals resulting in brain injury[36]. In this study, AD-group revealed signs of hippocampus exposure to oxidative stress; considerable rise in hippocampal MDA with a significant decrease in hippocampal TAC, which were consistent with a previous research in which reported that the reactive oxygen species (ROS(production can affect synaptic as well as non-synaptic neurons communication, resulting in nerve inflammation and cell death , eventually leading to neurodegeneration and loss of memory[37].

Chronic inflammatory disorders are exacerbated by oxidative stress as it induces damage, such as oxidized proteins and lipid peroxidation, leads to neurodegeneration, which is frequently observed in brain disorders[35]. Aluminum accesses the BBB and accumulates in many brain parts. Additionally, it induces formation of the free radicals resulting in brain injury[36]. In this study, AD-group revealed signs of hippocampus exposure to oxidative stress; considerable rise in hippocampal MDA with a significant decrease in hippocampal TAC, which were consistent with a previous research in which reported that the reactive oxygen species (ROS(production can affect synaptic as well as non-synaptic neurons communication, resulting in nerve inflammation and cell death, eventually leading to neurodegeneration and loss of memory[37].

Oxidative stress found in the AD group could account for the downregulation of acetylcholinesterase (AChE) and malondialdehyde (MAO). These findings are consistent with previous studies. As AD progresses, different types of neurons degenerate. Consequently, there is a large decrease in cholinergic neurons with a reduction in the acetylcholine hydrolyzing enzyme, AChE and choline acetyltransferase (ChAT), the rate-limiting enzyme that synthesizes Ach. However, AlCl3 significantly increased AChE activity in the hippocampus[38]. The marked high level of AChE activity by aluminum could be exacerbated by the interplay between the Al+3 cations and the anionic sites in the brain AChE[39]. Malondialdehyde is implicated in neuronal damage and the generation of H2O2, which is a major cause of oxidative stress. A radioenzymatic investigation discovered considerably decreased MAO-A's activity in the frontal cortical area of patients suffering from AD than in controls[40]. In addition, retinoic acid regulates MAO via a particular route. However, this system may be downregulated with aging, as retinoic acid signaling is diminished in the old brains or persons with cognitive decrease. However, increased activity of MAO-B in the platelets and brain of people complaining of neurodegenerative diseases, like Alzheimer's and Parkinson's disease was reported[41].

The MSCs and their derivatives secrete neurotrophic factors like brain-derived neurotrophic factor and vascular endothelial growth factor, leading to the synthesis of anti-inflammatory cytokines like interleukin-10 and transforming growth factor-β. Treatment with exosomes improves damaged neurological capacities and has a neuroprotective impact against oxidative stress in addition to increasing neurotic density in neurons[42]. The administration of CM or exosomes decreased the oxidative stress generated by AlCl3, resulting in cognitive enhancement (learning and working, spatial and recognition memory as detected by the previously described behavioral tests). However, exosomes significantly increased discrimination index, locomotor and anxiety behavior compared to CM[43]. These previous results match the results of the present study in which the CM-treated group spent significantly longer freezing and grooming duration than the control group. Additionally, the exo-treated group had a substantial drop in the number of crossed peripheral squares, with no significant decrease in rearing frequency. The Exo-treated group had significantly longer frozen time but with no significant increase in grooming duration.

This cognitive improvement in rats of treated groups may occur after oxidative stress is improved, resulting in a significant decrease in hippocampal MDA and a significant increase in hippocampal TAC in the CM and exosome groups when compared to the AD group, with no significant differences between the CM and Exo groups. Thus, both CM and exosomes lower hippocampus oxidative stress, which is in agreement with the results of previous researches[44].

The reduced oxidative stress in the treated groups could account for the restoration of AChE and MAO expression levels in the CM and Exo groups when compared to the AD groups. Both CM and exosomes maintained neuronal survival and plasticity, stimulate axonal regeneration and effectively prevent hippocampus neuronal and non-neuronal cell death. These findings are consistent with a previous study[44]. Interestingly, Exo-group significantly restored their levels compared to the CM-group.

AlCl3 caused significant histological alterations in the AD group, including neurodegeneration and neuron loss. Pyramidal neurons exhibited degeneration, including reduced cell bodies, intracytoplasmic vacuolations and organelle affection, particularly the rough endoplasmic reticulum. AlCl3-induced neurodegeneration may be caused by oxidative damage and chronic inflammation. Furthermore, the observation of dilated endoplasmic reticulum cisternae is the most well-characterized indicator of oxidative stress at the ultrastructural level[45].

Pyramidal neurons are cells with active protein synthesis but perish by apoptosis as a result of prolonged and intensive exposure to unfavorable stimuli (such as oxidative stress) or because of genetic abnormalities[46]. Caspase activation is a significant cause of the appearance of these dark cells, as well as their subsequent death. Inflammasomes can activate caspases, which leads to an increase in dark cells and, as a result, memory impairment[47].

In the current investigation, the AD group showed degeneration in the cytoplasm and evidence of degeneration in cytoplasmic organelles. There was a link between mitochondrial damage in AD and intrinsic mitochondria-mediated apoptosis caused by oxidative stress[48]. Furthermore, elevated Amyloid-β (Aβ) levels may contribute to mitochondrial dysfunction, either directly or indirectly. Mitochondria have a functioning □-secretase complex and amyloid-beta protein precursor, making them potential Aβ synthesis sites[49]. The Aβ can interplay with amyloid-beta binding alcohol dehydrogenase in mitochondria, increasing ROS production, activating caspase 3 and decreasing ATP[50]. Degenerative changes of nerve axons, detected as axonal segmentation and thinning, were identified in Bielschowsky's silver-stained sections, as well as the TEM findings, which revealed axoplasmic vacuolation and myelin sheath degeneration. Previous studies have connected increasing axonal degeneration in the early phases of AD, involving Aβ precipitation and tau hyperphosphorylation[51]. This, in turn, inhibits axonal transport, eventually leading to full transport blockage, axonal degeneration, synaptic disorder and axonal leaking[52].

In addition to axonal injury, AlCl3 produced myelin sheath degradation, as it was previously shown that the breakdown of white matter and myelination were among the first histological alterations in the rat model of AD[53].

In AD-group of the current study, intra-neuronal aggregations of argyrophilic neurofibrillary tangles (NFTs) were seen in cells from the CA1, CA4 and DG areas. NFTs developed as an accumulation of argyrophilic neurofibrils, which were primarily seen in neuronal cell bodies and the proximal parts of axons. It was formerly reported that AlCl3 caused

production of internal NFTs and extracellular amyloid proteins, which are considered the two hallmarks of AD[54]. Both toxic proteins were readily visible in stained sections of Bielschowsky's silver in this study, showing chronic inflammation that may have caused oxidative stress injury. NFTs' principal ingredient was revealed to be the microtubule-associated protein tau, which is generally present in axon's cytoplasm[55]. It appears aberrantly misfolded and abnormally hyperphosphorylated, which is caused by persistent inflammation and cellular stress of neurons described in AD and its extent is closely connected with the severity of neuronal dama. One of the NFT isoforms is the mature or fibrillar intraneuronal NFTs, which consist of aggregates of cytoplasmic filaments of tau that pushing the nucleus to the periphery of the cell body and frequently extend to damage the appearance of dendrites and the proximal segment of the axon[56]. They are particularly damaging to neurotransmitter transport and axonal integrity, resulting in functional impairment in AD[57].

Abnormal precipitate of Aβ protein in brain areas is commonly noticed in AD. Amyloid plaques are spherical aberrant extracellular accumulation and accumulation of the amyloid-β peptide (Aβ) with 40 or 42 amino acids (Aβ 40 and Aβ 42), which are typical results of APP processing. In normal settings, its physiological role is to modulate synaptic activity. In Alzheimer's disease, Aβ builds up into soluble oligomers that harm synapses and insoluble β-sheet pleated amyloid fibrils that form plaques. APs can be divided into two types: diffuse APs and dense core APs[58]. Some researchers documented that diffuse plaques are amorphous amyloid accumulates with poorly defined contours. While thick core plaques are made up of fibrillar amyloid deposits with compact cores. They are commonly detected in patients with AD and are related to synaptic loss. Their existence is typically linked to the existence of cognitive decline[59].

In this study, the administration of CM/Exo significantly improved the majority of the degenerative effects caused by AlCl3, including neuronal damage, NFTs, APs and axon damage. The CM/Exo-treated groups had a significantly lower number of deteriorated neurons than the AD group. However, the Exo-treated group had considerably decreased the amount of NFT cells if compared to the AD group.

MSCs-CM increased Aβ-phagocytosis, reducing Aβ plaques in AD mice models by increasing microglial phagocytic activity. Injection of MSCs-CM can prevent diabetes-induced neuronal degeneration in rats' hippocampus by lowering oxidative stress and apoptosis by enhancing antiapoptotic Bcl-2 expression and downregulating the proapoptotic Bax gene[60].

Interestingly, the Exo-treated group of the present study displayed a significant decrease in the number of degenerated cells and NFTs´ cells if compared to the CM-treated group. Conditioned media exosomes have neuroprotective effects against oxidative stress in aging brain and AD[61]. BM-MSC-derived exosomes supply functional micro-RNAs to brain cells, which increase cell persistence by lowering the activity of cell death genes, such as Bad, Bax and caspase-3. This resulted in neurotic remodeling and suppression of apoptosis, which in turn can ameliorate the functional recovery. MSC-derived exosomes also protect against amyloid-oligomer-induced oxidative stress and synaptic loss in hippocampus neurons[43].

The inflammatory cascade has a critical role in the progress of neurodegenerative disorders. TNF-α is a proinflammatory cytokine responsible for immunological dysfunction and inflammation in various tissues and organs[62]. In the current work; there was a significant increase in TNF-α level in AD-group, This matches the results of former studies proposed that AlCl3 selectively impacts macrophage activities and promotes the progress of brain damage[53].

Microglia are the 1ry immune cells of the CNS that respond rapidly to disturbances in brain homeostasis during stress, trauma or pathology while also facilitating synaptic plasticity, learning and memory. They play a critical role in clearing extracellular and intracellular Aβ and NFTs, protecting neuronal tissue in AD and reducing synaptotoxic Aβ oligomer diffusion[63]. Any defects in these functions have a stronger effect on disease progression and the pathogenic cascade of synaptic loss, neuronal death and brain damage evident in Alzheimer's disease. Activated microglia have 2 phenotypes: M1, which is typically activated and M2, which is alternately activated. M1 microglia produce high levels of pro-inflammatory cytokines such as IL-1β, IL-12, TNF-α and iNOS, which can accelerate CNS injury. M2 microglia respond to IL-4, IL-10, IL-13 and TGF-β, which have anti-inflammatory effects in AD[64].

In the current study, significantly increased M1 and decreased M2 microglia in AD-group. It was postulated that Aβ plaques activate microglia,

which respond to cerebral amyloidosis with a chronic pro-inflammatory response[65]. Alzheimer's disease is characterized by activated microglia, they are less ramified, thicker and have shorter processes. Neurotoxins and cytokines are released by Aβ-activated microglia, which leads to neurodegeneration[66].

Because Microglia produce inflammation in response to complement activation, phagocytose synapses, worsen tau pathology and can react proinflammatory to protein aggregates and dying neurons through the secretion of inflammatory mediators and play a significant role in complement-mediated synapse loss in AD[67].

Activated microglia; dark microglial, were observed in AD-group by TEM. These results were previously recorded and the authors suggested that Dark microglial cells exhibit ultrastructural characteristics of cells under oxidative stress[68]. In amyloid-β disease, cells show electron-dense cytoplasm and nucleoplasm, dilated endoplasmic reticulum and loss of heterochromatin. Oxidative stress also causes cellular shrinkage, which stimulates the accumulation of their cytoplasmic and nucleoplasmic contents e.g., lipids and proteins were demonstrated with osmium tetroxide, explaining why these cells seemed black in TEM. They were postulated to represent a subpopulation of hyperactive microglia caused by prolonged microglia activation, which became stressed as a result of their hyperactivity when faced with adaptive challenges. This resulted in abnormal synaptic connections and elevated phagocytic activity[69].

In the current work, the CM and exosomes treated groups demonstrated a substantial decrease in TNF-α levels, decreased M1 (+CD86) and increased M2 (+CD163) compared to the AD group. Consequently, MSC derivatives not only reduced the M1 phenotype but also enhanced the M2 phenotype, which subsequently regulates neuroinflammation, as previously documented[70]. In AD mouse model, treatment with MSCs-CM reduced the production of proinflammatory cytokines and oxidative-nitrosative stress indicators such IL-1β, TNF-α and iNOS. Furthermore, MSC-exosomes were related to the up-regulation of anti-inflammatory cytokines and the decrease of pro-inflammatory cytokines in vivo and in vitro, thus, modulating neuroinflammation[71].

Conditioned media activation of M2-type microglia has led to the production of mRNA encoding BDNF, a neurotrophins that has a role in synaptic enhancement as well as memory formation in the hippocampus's adult. In AD mouse model, MSCs-exosomes activate M2 microglial cells, resulting in more synthesis of neprilysin and insulin-degrading enzymes. These enzymes play a vital role in Aβ decomposition[72]. Interestingly, the Exo-treated group demonstrated a significant increase in M2 (anti-inflammatory), but not in CD-86 (proinflammatory, M1) microglial as compared to the CM-group.

The CM and Exo groups had hyperactive dark microglia, which were recognized by electron dense cytoplasm and undistinguished nuclei. This could be explained by the persistent oxidative stress and AP accumulation, which could not be eliminated by their administration.

Astrocytes are the most numerous type of glial cells in the CNS and have several critical functions, such as metabolic effects, blood-brain barrier, maintenance of ionic balance, share in synaptogenesis, neurogenesis, synaptic transmission and ameliorate the effects on the neuronal microenvironment under different physiological conditions[73]. Pathological situations can trigger astrogliosis, a reactive state caused by brain injury, Aβ accumulation and inflammatory mediators such as nitric oxide and cytokines. The degree of astrogliosis changes is related to cognitive impairment[52].

The current investigation showed a substantial role for astrocyte activation in the AD group, as indicated by a considerable rise in GFAP immune-reactivity and increased astrocyte ramifications. Furthermore, TEM results revealed the existence of astrocytes with vacuolated cytoplasm engulfing myelin, less electron dense nuclear chromatin, dilated endoplasmic reticulum cisternae and damaged mitochondria. This agreed with Orta-Salazar and his coworkers[52].

When astrocytes are activated, they release cytokines and other chemicals involved in the inflammatory response, which are thought to significantly contribute to expanding brain damage. In addition, astrocytes in Alzheimer's disease can lead to Aβ deposition, worsening the disease's pathogenesis[74].

Both microglia and astrocytes are regarded as key components of the innate immune system due to their ability to create immunomodulators and express innate immunity-related receptors. Appropriate astrocyte-microglia crosstalk in illness is required for astrocytes to promote neuronal survival and function following acute injury. Microglia are the

first glial cells to activate and rapidly recruit to injured areas to phagocytose dead cells and debris. Then, astrocytes activate, releasing inflammatory mediators, upregulate GFAP and undergo structural changes resulting in astrogliosis, which might limit injury within the damaged area[75].

Activated microglia release cytokines such IL-1β, TNF-α and IL-6, which regulate astrocyte responses and reduce the P2Y1 receptor, allowing tissue remodeling and repair. Astrocytes release TGF-β, an anti-inflammatory mediator, which causes microglia to lower the expression of certain inflammatory mediators. Furthermore, it was shown that cytokine-activated astrocytes can enhance neurogenesis in adult mice in the sub-ventricular zone[76]. MSCs-CM and exosomes can improve astrocyte survival by GFAP downregulation. Also, MSCs-exosomes can generate anti-inflammatory effects by inhibiting reactive astrocytes and activated microglia[77]. These findings were consistent with our findings, which indicated that the CM and Exo groups had much lower levels of GFAP immunological reactivity than the AD group. Interestingly, the Exo-treated group demonstrated significant decreases in GFAP expression compared to the CM group.

The persistence of moderately activated astrocytes in the treated groups may improve AD by clearing Aβ plaque deposition, modulating immune and inflammatory processes through TGF-β and IGF-1 secretion and providing neuroprotective factors[78].

The DG is a unique portion of the hippocampus because it has the neurogenic stem cell niche, where they continue to create new neurons in the brain of the adults, in a distinct type of cellular plasticity known as adult hippocampal neurogenesis (AHN)[79].

In this present study, nestin immunohistochemical labeling, a marker for stem cells and progenitor cells, indicated a significant impairment of proliferation in hippocampal DG, indicating loss of hippocampal neurogenesis in AD.

One of the key alterations in AD seen in postmortem AD patients and animal models is impaired hippocampal neurogenesis. The onset of cognitive dysfunction implies that AHN impairment may be a causative factor in the cognitive decline that happens as AD disease progresses. AHN impairment also occurs before the accumulation of AD hallmarks[79].

The CM and Exo groups exhibited significant modulation in hippocampus neurogenesis. This is harmonious with researchers who reported that CM treatment in acute stroke may motivate the proliferation, migration and differentiation of endogenous neural progenitor cells, resulting in a considerable improvement in behavioral responsiveness. Furthermore, MSCs and MSC-derived exosomes can successfully boost neurogenesis in the subventricular zone and DG in the AD model by promoting neurogenesis, angiogenesis and synaptogenesis[80].

CONCLUSION

This experimental study proved a considerable therapeutic efficacy of CM and exosome treatments in the AD albino rat model. Both preserved the function and structure of neurons, reduced NFTs and APs formation, subsequently restored the hippocampal neuronal function, regulated astrocyte and microglial activity and enhanced the regenerative processes. However, exosome treatment was superior to CM regarding improvements of the cognitive function AChE and MAO, cellular structure (number of degenerated pyramidal neurons and the number of cells accumulating NFTs), astrogliosis, proliferation and microglial activation. This therapeutic effect was suggested to be mediated through CM/exosome antioxidant and anti-inflammatory effects and their promotion of resident neuronal stem cell proliferation. These results may pave the way in the future for further studies to ensure the clinical validity of exosome application for convenient and effective adjuvant therapy in AD patients.

CONFLICT OF INTEREST

There is no potential conflict of interest among the authors.

REFERENCES

1. Mandour, D.A., M. Bendary and A.E. Alsemeh, Histological and imunohistochemical alterations of hippocampus and prefrontal cortex in a rat model of Alzheimer like-disease with a preferential role of the flavonoid “hesperidin”. Journal of Molecular Histology, 2021. 52(5): p. 1043 - 1065.

2. Guo, T., *et al*., Molecular and cellular mechanisms underlying the pathogenesis of Alzheimer’s disease. 2020. 15(1): p. 1 - 37.

3. Tanaka, M., N. Török and L. Vécsei, Novel pharmaceutical approaches in dementia, in NeuroPsychopharmacotherapy. 2022, Springer. p. 2803 - 2820.

4. Alawdi, S.H., *et al*., Neuroprotective effect of nanodiamond in Alzheimer's disease rat model: a pivotal role for modulating NF-κB and STAT3 signaling. Molecular neurobiology, 2017. 54(3): p. 1906 - 1918.

5. Golianová, N., Cholinergic system as pharmacological target in Alzheimer's disease. 2018.

6. Martínez de Toda, I., *et al*., Altered redox state in whole blood cells from patients with mild cognitive impairment and Alzheimer's disease. 2019. 71(1): p. 153 - 163.

7. Breijyeh, Z. and R.J.M. Karaman, Comprehensive review on Alzheimer's disease: Causes and treatment. 2020. 25(24): p. 5789.

8. Teixeira, F.G. and A.J.J.N.r.r. Salgado, Mesenchymal stem cells secretome: Current trends and future challenges. 2020. 15(1): p. 75.

9. Squecco, R., *et al*., Bone marrow-mesenchymal stromal cell secretome as conditioned medium relieves experimental skeletal muscle damage induced by ex vivo eccentric contraction. 2021. 22(7): p. 3645.

10. Trzyna, A. and A.J.B. Banaś-Ząbczyk, Adipose-derived stem cells secretome and its potential application in "stem cell-free therapy". 2021. 11(6): p. 878.

11. Xunian, Z. and R.J.C.S. Kalluri, Biology and therapeutic potential of mesenchymal stem cell-derived exosomes. 2020. 111(9): p. 3100 - 3110.

12. Rifaai, R.A., *et al*., Neuroprotective effect of quercetin nanoparticles: A possible prophylactic and therapeutic role in alzheimer's disease. 2020. 107: p. 101795.

13. Ismail, O.I. and M.M.S. El-Meligy, Curcumin ameliorated low dose-Bisphenol A induced gastric toxicity in adult albino rats. Scientific Reports, 2022. 12(1): p. 10201.

14. El-Tahawy, A. and A.J.J.C.H. Ali, Possible Protective Effect of Bone Marrow-Mesenchymal Stem Cells (BM-MSCs) Against the Remote Liver Injury Induced by Renal Ischemia Reperfusion in Male Albino Rats. 2017. 8(484): p. 1 - 14.

15. Nakhaeifard, M., *et al*., Conditioned medium protects dopaminergic neurons in parkinsonian rats. 2018. 20(3): p. 348.

16. Sabry, D., *et al*., The effect of exosomes derived from mesenchymal stem cells in the treatment of induced type 1 diabetes mellitus in rats. 2020. 42: p. 1597 - 1610.

17. Othman, A., R. Mubarak and D.J.F. Sabry, Fibroblast growth factor-6 enhances CDK2 and MATK expression in microvesicles derived from human stem cells extracted from exfoliated deciduous teeth. 2018. 7.

18. Dominkuš, P.P., *et al*., PKH26 labeling of extracellular vesicles: Characterization and cellular internalization of contaminating PKH26 nanoparticles. 2018. 1860(6): p. 1350 - 1361.

19. Abdelwahab, S., *et al*., Comparative study between bone marrow mesenchymal stem cell and their conditioned medium in the treatment of rat model of Parkinsonism. 2021. 236(1): p. 440 - 457.

20. Hassan, R., *et al*., The prospective role of mesenchymal stem cells exosomes on circumvallate taste buds in induced Alzheimer's disease of ovariectomized albino rats:(Light and transmission electron microscopic study). 2020. 110: p. 104596.

21. Seibenhener, M.L. and M.C. Wooten, Use of the open field maze to measure locomotor and anxiety-like behavior in mice. JoVE (Journal of Visualized Experiments), 2015(96): p. e52434.

22. Kraeuter, A.-K., P.C. Guest and Z. Sarnyai, The Y-maze for assessment of spatial working and reference memory in mice. Pre-clinical models: Techniques and protocols, 2019: p. 105 - 111.

23. Lueptow, L.M., Novel object recognition test for the investigation of learning and memory in mice. JoVE (Journal of Visualized Experiments), 2017(126): p. e55718.

24. Alvarez-Mon, M.A., *et al*., Differential malondialdehyde (MDA) detection in plasma samples of patients with major depressive disorder (MDD): A potential biomarker. Journal of International Medical Research, 2022. 50(5): p. 03000605221094995.

25. Abdelghany, A.K., *et al*., Neuroprotective role of medicinal plant extracts evaluated in a scopolamine-induced rat model of Alzheimer's disease. 2022. 27(8): p. 773 - 783.

26. Pereira-Gómez, M., *et al*., Evaluation of SYBR Green real time PCR for detecting SARS-CoV-2 from clinical samples. Journal of virological methods, 2021. 289: p. 114035.

27. Ahmed, W.M., *et al*., Premna odorata extract as a protective agent on neurotoxic effect of aluminum: neurochemical, molecular and histopathological alterations. 2021. 28: p. 2146 - 2157.

28. Suvarna, K.S., C. Layton and J.D. Bancroft, Bancroft's Theory and Practice of Histological Techniques E-Book. 2018: Elsevier Health Sciences.

29. Litchfield, S. and Z. Nagy, New temperature modification makes the Bielschowsky silver stain reproducible. Acta neuropathologica, 2001. 101: p. 17 - 21.

30. Weil, M.-T., *et al*., Transmission electron microscopy of oligodendrocytes and myelin. Oligodendrocytes: Methods and protocols, 2019: p. 343 - 375.

31. Valdez, E.M., Estelita's Care Facility for Alzheimer's Patients in East Los Angeles. 2019: California State University, Long Beach.

32. Hamdan, A.M.E., *et al*., Neuroprotective effects of phytochemicals against aluminum chloride-induced Alzheimer's disease through ApoE4/LRP1, wnt3/β-catenin/gsk3β and TLR4/NLRP3 pathways with physical and mental activities in a rat model. Pharmaceuticals, 2022. 15(8): p. 1008.

33. Mathiyazahan, D.B., A.J. Thenmozhi and T.J.J.o.F.F. Manivasagam, Protective effect of black tea extract against aluminium chloride-induced Alzheimer's disease in rats: A behavioural, biochemical and molecular approach. 2015. 16: p. 423 - 435.

34. Chen, X., *et al*., Neuroprotective effects of ononin against the aluminium chloride-induced Alzheimer's disease in rats. 2021. 28(8): p. 4232 - 4239.

35. Popa-Wagner, A., *et al*., ROS and brain diseases: the good, the bad and the ugly. 2013. 2013.

36. Chen, X., *et al*., Neuroprotective effects of ononin against the aluminium chloride-induced Alzheimer's disease in rats. Saudi Journal of Biological Sciences, 2021. 28(8): p. 4232 - 4239.

37. Sathe, G., *et al*., Multiplexed phosphoproteomic study of brain in patients with Alzheimer's disease and age-matched cognitively healthy controls. Omics: a journal of integrative biology, 2020. 24(4): p. 216 - 227.

38. Hawash, Z.A.S., *et al*., Assessment of Anti-Alzheimer Pursuit of Jambolan Fruit Extract and/or Choline against AlCl3 Toxicity in Rats. Toxics, 2023. 11(6): p. 509.

39. Xu, W., *et al*., Biomimetic single Al-OH site with high acetylcholinesterase-like activity and self-defense ability for neuroprotection. Nature Communications, 2023. 14(1): p. 6064.

40. Behl, T., *et al*., Role of monoamine oxidase activity in Alzheimer's disease: an insight into the therapeutic potential of inhibitors. Molecules, 2021. 26(12): p. 3724.

41. Wołoszynowska-Fraser, M.U., A. Kouchmeshky and P.J.A.r.o.n. McCaffery, Vitamin A and retinoic acid in cognition and cognitive disease. 2020. 40: p. 247 - 272.

42. Kandeel, M., *et al*., Mesenchymal stem cell-derived extracellular vesicles: an emerging diagnostic and therapeutic biomolecules for neurodegenerative disabilities. Biomolecules, 2023. 13(8): p. 1250.

43. Aghaei, Z., *et al*., Neuroprotective Effect of Wharton's Jelly-Derived Mesenchymal Stem Cell-Conditioned Medium (WJMSC-CM) on Diabetes-Associated Cognitive Impairment by Improving Oxidative Stress, Neuroinflammation and Apoptosis. Stem Cells International, 2023. 2023.

44. Aghaei, Z., *et al*., Neuroprotective Effect of Wharton's Jelly-Derived Mesenchymal Stem Cell-Conditioned Medium (WJMSC-CM) on Diabetes-Associated Cognitive Impairment by Improving Oxidative Stress, Neuroinflammation and Apoptosis. Stem Cells International, 2023. 2023(1): p. 7852394.

45. Chen, Y., *et al*., Beneficial impact of cardiac heavy metal scavenger metallothionein in sepsis-provoked cardiac anomalies dependent upon regulation of endoplasmic reticulum stress and ferroptosis but not autophagy. Life Sciences, 2024. 336: p. 122291.

46. Zimatkin, S., Dark neurons of the brain. Neuroscience and behavioral physiology, 2018: p. 1 - 5.

47. Flores, J., *et al*., Therapeutic potential of Nlrp1 inflammasome, Caspase-1 or Caspase-6 against Alzheimer disease cognitive impairment. Cell Death & Differentiation, 2022. 29(3): p. 657 - 669.

48. Chen, S.-Y., *et al*., Traditional Chinese medicine: role in reducing β-amyloid, apoptosis, autophagy, neuroinflammation, oxidative stress and mitochondrial dysfunction of Alzheimer's disease. Frontiers in Pharmacology, 2020. 11: p. 497.

49. John, A. and P.H. Reddy, Synaptic basis of Alzheimer's disease: Focus on synaptic amyloid beta, P-tau and mitochondria. Ageing research reviews, 2021. 65: p. 101208.

50. Ye, Z., *et al*., Aβ-binding with alcohol dehydrogenase drives Alzheimer's disease pathogenesis: A review. International Journal of Biological Macromolecules, 2024: p. 130580.

51. Salvadores, N., C. Gerónimo-Olvera and F.A. Court, Axonal degeneration in AD: the contribution of Aβ and Tau. Frontiers in Aging Neuroscience, 2020. 12: p. 581767.

52. Rifaai, R.A., *et al*., Neuroprotective effect of quercetin nanoparticles: A possible prophylactic and therapeutic role in alzheimer's disease. Journal of Chemical Neuroanatomy, 2020. 107: p. 101795.

53. El-Beltagi, E.M., *et al*., Effect of Bone Marrow-Derived Mesenchymal Stem Cells on the Hippocampal CA1 Area of Aluminium Chloride-Induced Alzheimer's Disease in Adult Male Albino Rat: A Histological and Immunohistochemical Study. Egyptian Journal of Histology, 2022. 45(4): p. 968 - 985.

54. Almuhayawi, M.S., *et al*., The potential role of pomegranate and its nano-formulations on cerebral neurons in aluminum chloride induced Alzheimer rat model. Saudi journal of biological sciences, 2020. 27(7): p. 1710 - 1716.

55. Rawat, P., *et al*., Phosphorylated tau in Alzheimer's disease and other tauopathies. International Journal of Molecular Sciences, 2022. 23(21): p. 12841.

56. Srinivas, K., Amyloid Maturation Patterns in Alzheimer's Disease-Novel chemical imaging of Aβ and Tau pathology. 2023.

57. Verma, H., *et al*., Understanding the neuronal synapse and challenges associated with the mitochondrial dysfunction in mild cognitive impairment and Alzheimer's disease. Mitochondrion, 2023.

58. Salahuddin, P., *et al*., The role of amyloids in Alzheimer's and Parkinson's diseases. International Journal of Biological Macromolecules, 2021. 190: p. 44 - 55.

59. Lemke, G. and Y. Huang, The dense-core plaques of Alzheimer's disease are granulomas. Journal of Experimental Medicine, 2022. 219(8): p. e20212477.

60. Elshemy, M.M., *et al*., Antioxidative capacity of liver-and adipose-derived mesenchymal stem cell-conditioned media and their applicability in treatment of type 2 diabetic rats. Oxidative medicine and cellular longevity, 2021. 2021.

61. Zhang, W., *et al*., Astrocyte-derived exosomes protect hippocampal neurons after traumatic brain injury by suppressing mitochondrial oxidative stress and apoptosis. Aging (Albany NY), 2021. 13(17): p. 21642.

62. Suescun, J., S. Chandra and M.C. Schiess, The Role of Neuroinflammation in Neurodegenerative Disorders, in Translational inflammation. 2019, Elsevier. p. 241 - 267.

63. Viola, K.L. and W.L. Klein, Amyloid β oligomers in Alzheimer's disease pathogenesis, treatment and diagnosis. Acta neuropathologica, 2015. 129: p. 183 - 206.

64. Tang, Y. and W. Le, Differential roles of M1 and M2 microglia in neurodegenerative diseases. Molecular neurobiology, 2016. 53: p. 1181 - 1194.

65. Wang, W.-Y., *et al*., Role of pro-inflammatory cytokines released from microglia in Alzheimer's disease. Annals of translational medicine, 2015. 3(10).

66. Heneka, M.T., *et al*., Neuroinflammation in Alzheimer's disease. 2015. 14(4): p. 388 - 405.

67. Wen, L., D. Bi and Y. Shen, Complement-mediated synapse loss in Alzheimer's disease: mechanisms and involvement of risk factors. Trends in Neurosciences, 2023.

68. Bisht, K., *et al*., Dark microglia: a new phenotype predominantly associated with pathological states. Glia, 2016. 64(5): p. 826 - 839.

69. Nichols, M.R., *et al*., Inflammatory mechanisms in neurodegeneration. Journal of neurochemistry, 2019. 149(5): p. 562 - 581.

70. Pang, Q.-M., *et al*., Regulatory role of mesenchymal stem cells on secondary inflammation in spinal cord injury. Journal of Inflammation Research, 2022: p. 573 - 593.

71. Nazari, S., *et al*., Mesenchymal stem cells (MSCs) and MSC-derived exosomes in animal models of central nervous system diseases: Targeting the NLRP3 inflammasome. IUBMB life, 2023. 75(10): p. 794 - 810.

72. Rahbaran, M., *et al*., Therapeutic utility of mesenchymal stromal cell (MSC)-based approaches in chronic neurodegeneration: a glimpse into underlying mechanisms, current status and prospects. Cellular & Molecular Biology Letters, 2022. 27(1): p. 56.

73. Araki, T., Y. Ikegaya and R. Koyama, The effects of microglia-and astrocyte-derived factors on neurogenesis in health and disease. European Journal of Neuroscience, 2021. 54(5): p. 5880 - 5901.

74. Li, K., *et al*., Reactive astrocytes in neurodegenerative diseases. Aging and disease, 2019. 10(3): p. 664.

75. Burda, J.E. and M.V. Sofroniew, Reactive gliosis and the multicellular response to CNS damage and disease. Neuron, 2014. 81(2): p. 229 - 248.

76. Diniz, L.P., *et al*., Astrocytes and the TGF-β1 pathway in the healthy and diseased brain: a double-edged sword. Molecular neurobiology, 2019. 56: p. 4653 - 4679.

77. Hajinejad, M. and S. Sahab-Negah, Neuroinflammation: The next target of exosomal microRNAs derived from mesenchymal stem cells in the context of neurological disorders. Journal of cellular physiology, 2021. 236(12): p. 8070 - 8081.

78. Ogunmokun, G., *et al*., The potential role of cytokines and growth factors in the pathogenesis of Alzheimer's disease. Cells, 2021. 10(10): p. 2790.

79. Denoth-Lippuner, A. and S. Jessberger, Formation and integration of new neurons in the adult hippocampus. Nature Reviews Neuroscience, 2021. 22(4): p. 223 - 236.

80. Kim, J., *et al*., Mesenchymal stem cell therapy and Alzheimer's disease: current status and future perspectives. Journal of Alzheimer's Disease, 2020. 77(1): p. 1 - 14.

الملخص العربي

الحويصلات الخارج خلوية المشتقة من الخلايا الجذعية الوسيطة مقابل وسطها المكيف في تحسين حصين نموذج الجرذان لمرض الزهايمر. دراسة سلوكية، كيميائية حيوية، نسيجية، هستوكيميائية مناعية

دينا على ماهر عبد الدايم[١]، أميرة فتحي أحمد[١]، ولاء يحي عبد الظاهر[٢]، مروة إبراهيم عبد الحميد[٣]، فاطمة خليل[٤]، نشوة فتحي جمال الطحاوى[١]، سهام عبد الرؤوف عبد العليم[١]، سارة محمد نجيب عبد الحافظ[١]

[١]قسم الهستولوجي وبيولوجيا الخلية - [٢]قسم الفارماكولوجي الطبية - كلية الطب - جامعة المنيا

[٣]قسم الكيمياء الحيوية - كلية الطب البيطري - جامعة القاهرة

[٤]قسم رعاية وتنمية الثروة الحيوانية والداجنة - كلية الطب البيطري - جامعة بني سويف

الخلفية: مرض الزهايمر هو أكثر أنواع الخرف انتشارًا مؤخرا تم استخدام الوسط المكيف للخلايا الجذعية الوسيطة والحويصلات الخارج خلوية في عدد من الابحاث العلاجية.

الهدف من البحث: توضيح التغيرات السلوكية والكيميائية الحيوية والنسيجية والهستوكيميائية المناعية في قرن آمون للجرذان البيضاء بعد تحفيز مرض الزهايمر فيها وتقييم دور الوسط المكيف المشتق من الخلايا الجذعية الوسيطة مقابل الحويصلات الخارج خلوية في نموذج مرض الزهايمر بالجرذان البيضاء.

طريقة البحث: استخدم عشرة جرذان لتحضيرالوسط المكيف المشتق من الخلايا الجذعية الوسيطة والحويصلات الخارج خلوية واثنين وثلاثين جرذا في هذه الدراسة قسمت إلى أربع مجموعات؛ المجموعة الضابطة ومجموعة مرض الزهايمر والمجموعة المعالجة بالوسط المكيف والمجموعة المعالجة بالحويصلات الخارج خلوية، وأجريت للجرذان اختبارات سلوكية، واستخدمت أنسجة الحصين لإجراء التقييمات البيوكيميائية والنسيجية والهستوكيميائية المناعية.

نتائج البحث: أظهرت مجموعة جرذان نموذج الزهايمر تغيرات سلوكية، كما أظهرت الجرذان تغيرات فى مالونديالدهيد الحُصيني وعامل نخر الورم وانخفاض تنظيم السعة الكلية لمضادات الأكسدة وأستيل كولين استريز وأوكسيديز أحادي الأمين، ومن الناحية المجهرية، أظهر الحصين خلايا عصبية متحللة بالإضافة إلى تشابكات ليفية عصبية محبة للفضة وتكوين لويحات أميلويد. أظهرت المجموعات المعالجة والمجموعة المعالجة بالوسط المكيف والإكسوسومات تحسنًا كميائيا وظيفيًا وبنائيا مع انخفاض التشابكات الليفية العصبية المحبة للفضة ولويحات الأميلويد. وكان العلاج بالإكسوسومات متفوقًا على المجموعة المعالجة بالوسط، كما أنها تعمل على تحسين وظائف الخلايا العصبية وتنظيم أنشطة الخلايا النجمية والخلايا الدبقية الصغيرة وتعزيز التغيرات التجديدية.

الاستنتاجات: تجريبياً في هذا العمل، قلل الوسط المكيف للخلايا الجذعية والجزيئات الخارجية من التغيرات التنكسية

والكيميائية الحيوية والنسيجية المناعية المرتبطة بمرض الزهايمر في حصين في الجرذان البيضاء مع تأثير أفضل لعلاج الجزيئات الخارج خلوية، ولذلك قد تمهد هذه النتائج لاستخدامها في المستقبل كعلاج فعال لمرضى الزهايمر.